New Journal and we have not received input yet 25 (2021) 101024

Contents lists available at ScienceDirect

Thermal Science and Engineering Progress

journal homepage: www.sciencedirect.com/journal/thermal-science-and-engineering-progress

# Pool boiling review: Part I – Fundamentals of boiling and relation to surface design

M.M. Mahmoud [a], T.G. Karayiannis [b,*]

[a] Zagazig University, Faculty of Engineering, Zagazig 44519, Egypt
[b] Brunel University London, Department of Mechanical and Aerospace Engineering, Uxbridge UB8 3PH, UK

ARTICLE INFO

*Keywords:*
Pool boiling
Bubble incipience
Growth
Departure
Enhancement

ABSTRACT

The pool boiling process is one of the most effective heat transfer modes capable of transferring large amounts of heat with small temperature difference between the heated surface and the fluid. In addition, fundamental knowledge of pool boiling processes is the starting point of flow boiling research and applications. It is therefore no surprise that it has been, and still is, the subject of extensive research globally for quite some time and a critical analysis is now required in order to move forward with enhanced surface designs. The current on-going research focuses on the understanding of boiling fundamentals including bubble generation, growth and bubble dynamics. In this context, fluid-surface interaction is critical. In the first part of this two-part paper we present the factors and parameters affecting the above, starting with the criteria for gas/vapour entrapment, nucleation site stability and the superheat required for heterogeneous nucleation. The models predicting the incipience superheat are critically described, classified into phase instability and superheated boundary-layer based models. This first part includes bubble growth and departure models, elucidating the effect of surface topology and wettability that can inform and facilitate the design of enhanced surfaces that are presented in Part II [10]. Three fluids of industrial interest, i.e. FC-72, HFE7100 and water were used through the discussion, as examples, to represent low and high surface tension fluids and help the understanding of surface-fluid interactions and relation to possible heat transfer enhancements.

## Introduction

Nucleate pool boiling has a wide range of applications such as cooling of nuclear reactors, evaporators in thermal desalination and refrigeration systems, chemical industries and more recently in electronics cooling, to mention just a few. It is one of the most efficient heat transfer regimes in which large amounts of heat can be dissipated from a heated surface with small changes in temperature. The heat transfer mechanisms in this boiling regime are illustrated in Fig. 1 and summarized as follows: (i) natural convection (wall to liquid) at low heat fluxes when there is no bubble coalescence and interaction, (ii) micro-convection induced by the liquid motion resulting from bubble growth, (iii) evaporation of the liquid microlayer trapped underneath the bubble, (iv) evaporation from the superheated thermal layer around the bubble, (v) transient heat conduction during the rewetting process that follows bubble departure plus (vi) forced convection resulting from bubble agitation in the liquid bulk. These mechanisms are difficult to segregate and the contribution of each mechanism may vary with the fluid and heat flux (wall superheat). For example, Moghaddam and Kiger [1] reported 16.3 – 28.8 % contribution from the microlayer evaporation in FC-72 while Narayan et al. [2] reported 66 % contribution in water. Heat transfer rates in pool boiling depend, in a complex way, on the fluid and surface characteristics. And, although pool boiling has been investigated for many years, there is still scatter in the prediction of bubble growth rate, bubble departure diameter and frequency, heat transfer coefficient (HTC) and critical heat flux (CHF) due to the lack of understanding of the complex effects of surface microstructure and fluid properties. It is worth mentioning that the effect of surface microstructure depends on system pressure. In high pressure systems, (e.g. power generation, refrigeration and air conditioning, thermal desalination), the range of active nucleation sites extends to include cavities of nanometer size. For example, using the Hsu [3] model, the minimum cavity diameter for water at 1 bar and 15 K superheat is 4.4 μm while it decreases to 0.22 μm at 20 bar. This cavity size is very common in conventional engineering surfaces. It means that wide range of cavities can be activated at high pressures (higher heat transfer rates) and thus surface modification may not be economic at high system

* Corresponding author.
*E-mail addresses:* mbasuny@zu.edu.eg (M.M. Mahmoud), tassos.karayiannis@brunel.ac.uk (T.G. Karayiannis).

https://doi.org/10.1016/j.tsep.2021.101024
Received 14 May 2021; Accepted 22 July 2021
Available online 27 July 2021

**Nomenclature**

| | |
|---|---|
| $a$ | Empirical constant in Eq. (1) |
| $b$ | Empirical exponent in Eq. (1) |
| $c_{pl}$ | Liquid specific heat, [J/kg K] |
| $c_w$ | Wall specific heat, [J/kg K] |
| $D_c$ | Cavity mouth diameter, [m] |
| $D_d$ | Bubble departure diameter, [m] |
| $f$ | Bubble generation frequency, [Hz], ratio of bubble embryo radius to cavity radius, [-] |
| $F_s$ | Surface tension force, [N] |
| $g$ | Acceleration due to gravity, [m/s$^2$] |
| $H$ | Cavity depth, [m] |
| $h_c$ | Capillary rise length, [m] |
| $h_{nc}$ | Natural convection heat transfer coefficient, [W/m$^2$ K] |
| $h_{tp}$ | Two-phase heat transfer coefficient, [W/m$^2$ K] |
| $h_{fg}$ | Latent heat, [J/kg] |
| K | Empirical parameter in Eq. (1) |
| $k_l$ | Liquid thermal conductivity, [W/m K] |
| $k_w$ | Wall thermal conductivity, [W/m K] |
| $La$ | Capillary length, [m] |
| $P$ | Pressure, [Pa] |
| $Ja$ | Jackob number, [-],$\rho_l c_l \Delta T_{sup}/\rho_v h_{fg}$ |
| $P_c$ | Capillary pressure, [Pa] |
| $Pr$ | Liquid Prandtl number, [-] |
| $q$ | Heat flux, [W/m$^2$] |
| $r_P$ | Pore radius, [m] |
| $r$ | Radius, [m] |
| $r_b, R$ | Bubble radius, [m] |
| $r_c$ | Cavity radius, [m] |
| $r_e$ | Embryo radius, [m] |
| $r_e^*$ | Critical bubble embryo radius, [m] |
| $S$ | Dimensionless surface parameter, [-] |
| $s$ | Slope of the vapour-pressure curve, [Pa/K] |
| $T$ | Temperature, [K] |
| $T_c$ | Critical temperature, [K] |
| $T_{sat}$ | Saturation temperature, [K] |
| $T_L$ | Liquid temperature, [K] |
| $T_b$ | Bubble temperature, [K] |
| $T_w$ | Wall temperature, [K] |
| $\Delta T_{sub}$ | Liquid sub-cooling, [K] |

*Abbreviations*

| | |
|---|---|
| CHF | Critical Heat Flux |
| HTC | Heat Transfer Coefficient |
| IGBT | Insulated Gate Bipolar Transistor |
| MLE | Micro Layer Evaporation |
| PCB | Printed Circuit Board |
| $\Delta T_{sup}$ | Wall superheat, [K] |
| $t$ | Time, [s] |
| $t_w$ | Waiting time, [s] |
| $V$ | Volume, [m3] |
| $v$ | Specific volume, [m$^3$/kg] |
| $v_{fg}$ | Liquid to vapour specific volume change, [m$^3$/kg] |
| $x^*$ | Liquid penetration depth in the cavity, [m] |
| $y_b$ | Bubble height, [m] |

*Greek symbols*

| | |
|---|---|
| $\alpha_w$ | Wall thermal diffusivity, [m$^2$/s] |
| $\alpha$ | Liquid thermal diffusivity, [m$^2$/s] |
| $\beta$ | Cavity cone half-angle, [deg] |
| $\beta_L$ | Volumetric thermal expansion coefficient, [1/K] |
| $\gamma$ | Parameter in Eq. (6) |
| $\delta_{th}$ | Thermal boundary layer thickness, [m] |
| $\varepsilon$ | Empirical parameter in Eq. (1) |
| $\theta$ | Contact angle, [deg] |
| $\theta_e$ | Static equilibrium contact angle, [deg] |
| $\theta_{ap}$ | Static apparent contact angle, [deg] |
| $\theta_d$ | Dynamic contact angle, [deg] |
| $\theta_{da}$ | Dynamic advancing contact angle, [deg] |
| $\theta_{dr}$ | Dynamic receding contact angle, [deg] |
| $\theta_{crit}$ | Critical contact angle in Eq. (8), [deg] |
| $\mu_l$ | Liquid dynamic viscosity, [Pa. s] |
| $\nu$ | Liquid kinematic viscosity, [m$^2$/s] |
| $\rho_l$ | Liquid density, [kg/m$^3$] |
| $\rho_v$ | Vapour density, [kg/m$^3$] |
| $\rho_w$ | Wall density, [kg/m$^3$] |
| $\sigma$ | Surface tension, [N/m] |
| $\sigma_{lv}$ | Liquid-vapour surface tension, [N/m] |
| $\sigma_{sv}$ | Solid-vapour surface tension, [N/m] |
| $\sigma_{ls}$ | Liquid-solid surface tension, [N/m] |
| $\varphi$ | Bubble shape angle in Eq. (7), [deg] |
| $\psi$ | Cavity mouth angle, [deg], parameter in Eq. (5) and Eq. (6) |
| RLE | Relaxation Layer Evaporation |
| TBL | Thermal Boundary Layer |
| TD | Temperature Deviation |
| TOS | Temperature Overshoot |
| TPL | Three Phase Contact Line |

operating pressures. On the contrary, in low pressure system applications, few nucleation sites could be active and therefore there is a need for surface modification to increase the number of active nucleation sites and consequently enhance the heat transfer rates. One example of these systems is electronics cooling which attracted a lot of research and was the focus of many researchers in the last twenty years. The challenge in electronics cooling is that the advances in technology resulted in the dissipation of huge amounts of heat from a small chip. Karayiannis and Mahmoud [4] discussed the challenges in thermal management of electronics equipment and reported that the average heat flux in computer chips is expected to reach 2 – 4.5 MW/m$^2$ with local hot spots 12 – 45 MW/m$^2$ while in insulated gate bipolar transistor modules (IGBT) the predicted value is 6.5 – 50 MW/m$^2$at the chip level. These heat fluxes are beyond the capability of existing conventional cooling techniques, e.g. air cooling and heat pipes.

Pool boiling has been used in electronics cooling through immersion cooling in which the printed circuit boards (PCBs) are directly immersed in a dielectric liquid. One limitation is that dielectric liquids are highly wetting, the latent heat is small, and the surface of the PCBs is usually smooth with restrictions on surface modifications. This resulted in large wall superheat at boiling incipience, i.e. the chip may become overheated before boiling starts, low heat transfer rates and critical heat flux (CHF). Thus, other techniques, such as on-chip cooling in which the heat sink is attached to the chip, emerged as a viable option, e.g. thermosyphon is one example. With on-chip cooling, it was possible to apply a wide range of surface modifications to the boiling surface to reduce the boiling incipience superheat and enhance the heat transfer rates and CHF. Additionally, it allowed the use of a wide range of fluids including water. Thus, more research was directed towards heat transfer enhancements by surface modification using various techniques which produced surfaces with complex microstructure. This research has been reviewed recently by many researchers, see for example [5 –9]. Mori and Utaka [5] reviewed the enhancement of CHF by surface modification and concluded that the CHF can be enhanced by increasing the number of nucleation sites, improving the wettability and capillary wicking, separation of the liquid and vapour pathways. Capillary wicking means

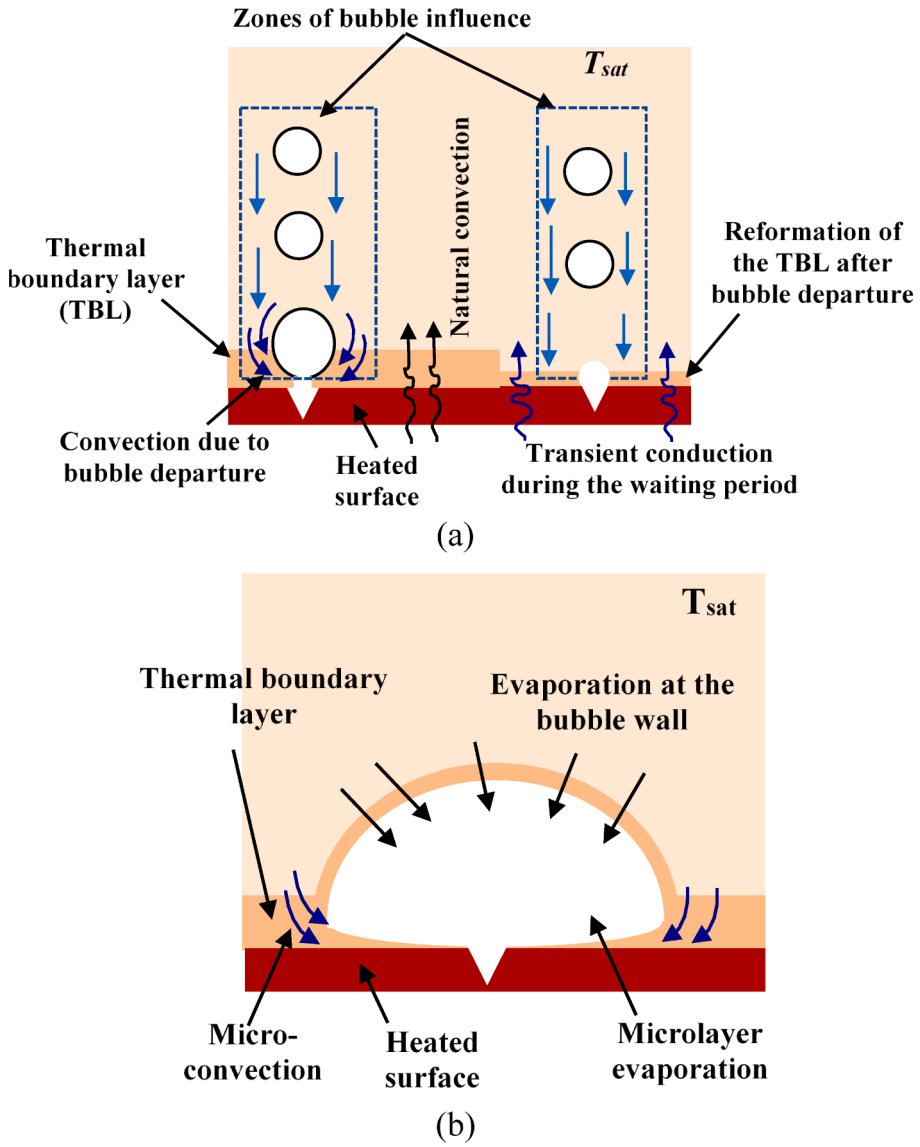


**Fig. 1.** Heat transfer mechanisms in pool boiling, (a) natural convection, bubble agitation and transient conduction during rewetting and reformation of the thermal boundary layer (TBL), and (b) micro-convection, microlayer evaporation and evaporation from the thermal layer around the bubble.

liquid flow laterally inside the porous structure due to capillary pressure force $P_c = 2\sigma cos\theta / r_P$ where $r_P$ is the pore radius. Additionally, they reported that the existing prediction models still need more validation and there is a need to conduct durability tests for the enhanced surfaces, i.e. surface aging. Finally, it was recommended that significant heat transfer enhancements are possible in surfaces with porous structure and large capillary force. Liang and Mudawar [6] classified the passive enhancement techniques into macroscale, microscale, nanoscale, hybrid scale and hybrid wettability. It was concluded that although there is a large number of studies on enhanced surfaces, there is still a scarcity of databases to establish the surface design in terms of fluid, surface material, surface size, orientation, structure pattern, scale (nano or micro) and operating pressure. Sajjad et al. [7] reviewed the boiling performance of what they referred to dielectric and highly wetting liquids on enhanced surfaces. They classified the enhanced surfaces into ID surfaces (surfaces that enhance either CHF or HTC) and 2D surfaces (surfaces that enhance CHF and HTC). It was concluded that (i) the high incipience superheat with dielectric liquids is due to the low surface tension and the poor thermophysical properties, (ii) the HTC can be enhanced by increasing the number of active nucleation sites, high surface porosity and thermal conductivity and ease of bubble detachment, (iii) the CHF can be enhanced by separating the liquid and vapour pathways, reduction in flow resistance, increased wettability and capillary wicking, and suppression of bubble coalescence (mushroom bubbles), (iv) boiling surfaces should be designed carefully to avoid the poor performance, e.g. coating thickness should be smaller than a critical value to reduce the thermal resistance. In other words, each enhancement technique should be optimized first before it becomes commercialized. Li et al. [8] classified the surface enhancement techniques into passive and active. The passive techniques include the surface modification by creating a structure such as fins, coating, nanofluid deposition while in what they called “active techniques”, the surfaces can adapt their structure and wettability during the boiling process which was called “smart surfaces”. They reported that the smart surfaces are promising but still are very challenging. Mehralizadeh et al. [9] conducted a review on the effect of surface enhancements on HTC, CHF and bubble dynamics. It was recommended that the best way to enhance the heat transfer is to use nanofluids along with surface structuring, which was attributed to the effect of the deposited nanoparticles on the surface.

From the past studies, the following comments can be summarized as follows: (i) All studies agreed on that the heat transfer performance (CHF and HTC) can be enhanced using a wide range of surface modification

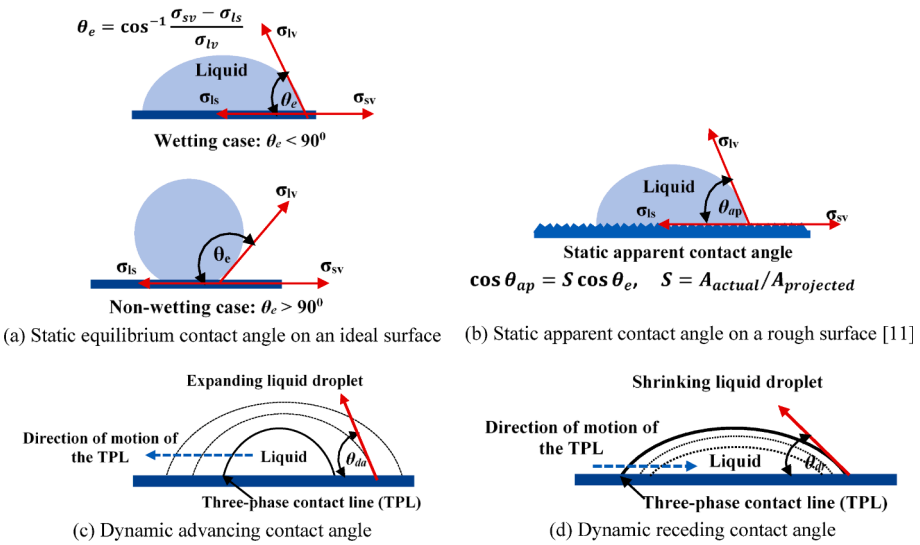


**Fig. 2.** Schematic drawing for the common definitions of equilibrium, static and dynamic contact angle.

techniques. (ii) The mechanisms of heat transfer and critical heat flux were discussed in most studies qualitatively without verification. In fact, inferring the heat transfer mechanism(s) in surfaces with random microstructure is very difficult. Verification of the heat transfer mechanisms requires the design and test of surfaces with artificial nucleation sites with known cavity size, geometry and pattern distribution, which is lacking in literature. The lack of research on surfaces with artificial cavities could be due to limitations in the manufacturing process, especially for metallic substrates. With artificial nucleation sites, it will be possible to understand several fundamental issues and optimize the surface parameters. (iii) There is a large scatter in the published data even for the same fluid, surface material and surface enhancement technique and the reasons of this scatter are not discussed. (iv) In most studies, the surface microstructure was designed randomly without adopting any design criteria. (v) Despite the large number of surface enhancement techniques, there is no general conclusion on the best fluid-surface structure and the best surface modification technique.

Thus, based on the above, the current paper is an attempt to understand the reasons behind the scatter in the published heat transfer data on plain and enhanced surfaces, through a critical assessment and new analysis of proposed models. This will remove inconsistencies in interpreting the fundamental concepts and help researchers apply this knowledge in surface design for improved heat transfer rates during boiling. We have used examples of low surface tension – low latent heat (FC-72, HFE7100) and high surface tension-high latent heat (water) fluids to enable critical appraisal of the work presented and its relation to heat transfer enhancement. The discussion will be limited only to boiling on horizontal upward facing flat surfaces and pure liquids at atmospheric pressure. The proposed passive enhancement techniques and the performance of the selected two fluids (FC-72 and water) on copper and silicon substrates will be discussed in Part II [10], which is published as a separate paper. Part I of the paper is organized as follows: section 2 presents the fundamentals of heterogeneous nucleation theories. Section 3 reviews the bubble dynamics and compares the different prediction models. The conclusions and recommendations are summarized in the last section.

## Heterogeneous nucleation

Heterogeneous nucleation is defined as the phenomenon of bubble generation (bubble initiation, growth, and departure) from a heated surface. It is a complex phenomenon affected by many factors such as surface microstructure, wettability, local thermal conditions, system pressure, material, and fluid thermophysical properties. Understanding the effect of these factors is very essential for the design of boiling surfaces. This section sheds some light on the fundamentals of heterogeneous nucleation to help understand the heat transfer performance of enhanced surfaces published in Part II [10].

### *Gas/vapour entrapment criteria*

It is commonly agreed that bubbles nucleate from pre-existing gas nuclei entrapped within the surface cavities. In other words, cavities that cannot trap gas may not be active nucleation sites. Thus, to design a boiling heat transfer surface, there is a need for design criteria to assure that a cavity with a certain geometry can trap gas. Because gas entrapment depends mainly on wettability, it would be useful to start with the definition of the various wettability contact angles. Wettability is a complex phenomenon and has been studied extensively. The aim of this section is not to review the topic of wettability but only the definition of contact angle will be given before discussing the gas entrapment criteria. Fig. 2 depicts a schematic drawing illustrating the definition of contact angle based on a liquid droplet sitting on a flat surface with the angle measured in the liquid side. The static equilibrium contact angle ($\theta_e$), see Fig. 2a for wetting and non-wetting case, is the angle formed on ideal surfaces, i.e. surfaces of homogeneous chemical composition and zero roughness. Static means that the angle is measured when the velocity of the three-phase contact line (TPL) becomes zero (stationary droplet). Because engineering surfaces are not ideal, the measured static contact angle on engineering surfaces are smaller than the equilibrium contact angle and is called the apparent static contact angle ($\theta_{ap}$). Fig. 2b shows the relation between the equilibrium contact angle and the apparent static contact angle given by Wenzel [11]. It depends on the dimensionless surface parameter ($S$), which is the wetted area of the rough surface divided by the projected area of the surface, i.e. $S > 1$. It indicates that the apparent static contact angle decreases as the roughness parameter increases, increasing the wettability. Fig. 2c depicts the definition of the dynamic advancing contact angle ($\theta_{da}$) which is defined as the angle measured when the TPL moves in the outward direction towards the vapour or gas (wetting mode), i.e. measured when the droplet expands by injecting more liquid into the droplet. When the TPL moves in the inward direction towards the liquid side (de-wetting mode when the droplet shrinks by withdrawing liquid from the droplet), the angle formed is called the dynamic receding contact angle ($\theta_{dr}$). It is worth mentioning that the dynamic contact angle (advancing and receding) is larger than the static contact angle and is a complex

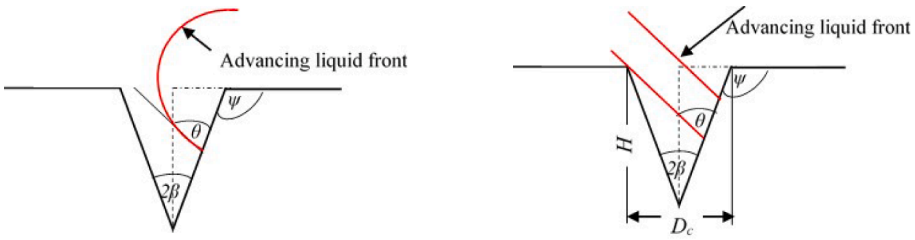


**Fig. 3.** Gas entrapment according to (a) Bankoff [12] and (b) Lorenz [13].

parameter because it depends strongly on the velocity of the TPL. Additionally, the advancing contact angle is usually larger than the receding contact angle and the difference is called contact angle hysteresis ($\theta_{da} - \theta_{dr}$).

Bankoff [12] and Lorenz [13] proposed that for a conical cavity to trap gas, the contact angle should be greater than the cavity cone angle, i.e. $\theta > 2\beta$. This criterion was based on the gas displacement by the advancing liquid front moving towards the cavity, see Fig. 3. They ignored the contact angle hysteresis and surface roughness, i.e. static and dynamic contact angles are equal. Tong et al. [14] recommended the same criterion but using the dynamic advancing rather than the static contact angle, $\theta_{da} > 2\beta$. As mentioned above, the dynamic advancing contact angle is always greater than the static contact angle. This means that cavities designed based on the dynamic contact angle will trap more gas than those designed based on the static contact angle. Thus, it may be concluded that cavities should be designed based on the static contact angle (the worst-case scenario) because the amount of trapped gas is expected to be larger if the dynamic motion of the TPL was taken into account (dynamic contact angle). Another reason is that the static contact angle is easy to measure compared to the dynamic contact angle, which makes surface design easier. Winterton [15] reported that, gas entrapment is not possible for wetting liquids ($\theta < 90^0$) because mechanical and thermal equilibrium require that the liquid–vapour interface inside the cavity must be concave in the liquid side when the surface temperature is significantly below the saturation temperature. Thus, the gas entrapment criterion was thought to be such that the dynamic advancing contact angle should satisfy the condition $\theta_{da} > 90 + \beta$. Cornwell [16] proposed a trapping criterion based on the contact angle hysteresis, which was attributed to the effect of micro roughness inside the cavity. The entrapment criterion was the same as that given by Winterton [15] but included the effect of surface roughness on the dynamic advancing contact angle. This criterion can be written in terms of the static contact angle (on a smooth surface), the cavity cone angle ($2\beta$) and the surface parameter ($S$) as:$\theta > 90 + \beta - cos^{-1}(1/S)$.

Wang and Dhir [17] conducted a thermodynamic analysis (minimization of the Helmholtz free energy) for a large droplet sitting on top of a cavity. Gas entrapment was deemed to occur when the Helmholtz free energy function exhibits a minimum. Accordingly, it was concluded that for conical, circular, and sinusoidal cavities to trap gas, the static contact angle should satisfy the condition $\theta > \psi$, where $\psi$ is the cavity mouth angle, see Fig. 3 above. For conical cavities, this condition is equivalent to $\theta > 90 + \beta$, which means that wetting liquids with $\theta < 90$ cannot trap gas. It is worth mentioning that the quantity of the entrapped gas does not affect only the bubble initiation but also can cause boiling hysteresis. For example, Shi et al. [18] discussed the mechanisms of hysteresis in nucleate pool boiling and reported the following two types: (i) temperature overshoot (TOS) hysteresis at boiling incipience, (ii) temperature deviation (TD) hysteresis in the region of transition from partial to fully developed nucleate boiling. The mechanism of TOS hysteresis was related to the quantity of the entrapped gas. If the cavities trap large amount of gas at the beginning (the first bubble ebullition cycle), the TOS hysteresis can be avoided. The TD hysteresis depends on the number and distribution of cavities that cannot trap gas (flooded cavities) but can be activated by the neighbor active cavities, i.e. displacement of the liquid from the cavity by the advancing vapour front. The flooded cavities can be activated by the advancing vapour front if the contact angle $\theta > \pi - 2\beta$. Because the cavity cone angle ($2\beta$) is small in most engineering surfaces, this condition is corresponding to $\theta > 90$ (hydrophobic/superhydrophobic case). This type of hysteresis is rarely encountered with highly wetting liquids which cannot satisfy this condition, i.e. cavities cannot be activated by the neighbour cavities. It can be concluded that boiling incipience hysteresis, which is very common with highly wetting liquids, may be considered as an indicator of gas entrapment in the surface cavities.

For design purpose, it is useful to present the gas entrapment criteria in terms of the cavity aspect ratio (depth/diameter) and static contact angle, especially for the design of surfaces with artificial cavities. This aspect ratio is the minimum required for cavities to trap gas. To do so, the advancing liquid front was assumed to be flat as adopted by Lorenz [13] in Fig. 3 (b) and the cavity depth was estimated from the relation: $\tan\beta = D_c/2H$ for conical cavities. Fig. 4 depicts the static contact angle

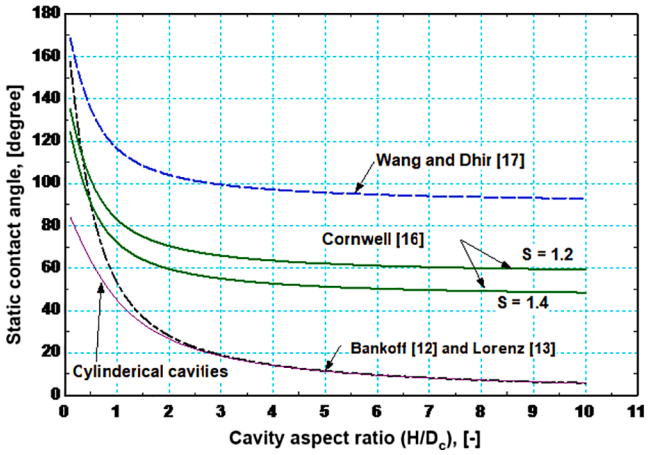


**Fig. 4.** The relation between static contact angle and the minimum conical cavity aspect ratio required for gas entrapment. A curve for cylindrical cavities is also included.

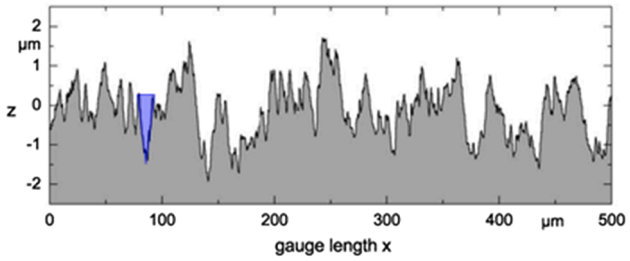


**Fig. 5.** Roughness profile for a sandblasted copper surface, Gorenflo et al. [19]. The shaded triangle shows a cavity with aspect ratio 4.67 and cavity cone angle about $6.1^0$.

versus the cavity aspect ratio predicted using the abovementioned criteria. The figure indicates that highly wetting liquids such as refrigerants (small contact angles), require cavities with large aspect ratios compared to non-wetting liquids. The large aspect ratio cavities may exist in most engineering surfaces with natural random roughness. For example, it is very common to measure peak to valley values of about 1 μm or larger and cavity radius of about 0.1 μm, which gives an aspect ratio of 5. Fig. 5 depicts a surface roughness profile measured for a copper surface prepared by sandblasting and quoted from Gorenflo et al. [19]. It shows that the aspect ratio is about 4.67 and the cavity cone angle is about $6.1^0$. It is worth noting that the criterion by Cornwell [16] is similar to that given by Wang and Dhir [17] when the surface parameter $S = 1$. Fig. 4 also includes a curve for cylindrical cavities, which was calculated using the same method ($\tan\theta = D_c/H$). It is obvious that this curve is coincident with Bankoff [12] and Lorenz [13] for small contact angle and gives slightly lower aspect ratio at higher contact angle. This means that Bankoff and Lorenz criteria are also applicable for the design of cylindrical cavities.

All the aforementioned criteria were based on theoretical analysis and are difficult to validate experimentally. Thus, there is a scarcity of experimental studies on the validation of gas entrapment in cavities. Pesse et al. [20] studied experimentally the effect of static contact angle and cavity geometry (depth, mouth width, cavity angle) on gas entrapment in closed-end rectangular microchannels. The channels were fabricated on silicon substrate to simulate the surface cavities with cross section 9 × 5 μm, 19 × 15 μm, 38 × 24 μm, 56 × 42 μm and depth 50, 150 and 500 μm. The measured contact angle covered a wide range, but it was less than $90^0$ (in the wetting range). It was found that all cavities were able to trap gas although the cavity has sharp mouth with cavity mouth angle (ψ) of $90^0$, which is against the criterion given by [15–17]. All the above criteria can be roughly validated in a simple manner using the simple capillary rise equation (penetration) in microstructure. If the microstructure was approximated as micro-holes of radius $r_p$, the capillary rise can be given as: $h_c = 2\sigma\cos\theta/\rho_l g r_P$. For $\theta \geq 90^0$, the capillary rise will be zero when the angle is $90^0$ and negative when the angle is above $90^0$ for all values of cavity radius i.e. no liquid penetration into the cavity and gas entrapment will occur regardless of the cavity size. In other words, all cavities in hydrophobic surfaces can trap gas, which is similar to the conclusion by [15–17]. On the contrary, for hydrophilic surfaces, the capillary rise equation predicts that the cavities will be partially filled with liquid and the quantity of the trapped gas will depend on the contact angle and cavity radius. If water was taken as an example at room temperature, cavity radius of 1 μm, and $\theta = 10^0$, the capillary penetration depth will be about 14.5 μm (aspect ratio = 7.2). This means that the cavity depth should be greater than 14.5 μm for the cavity to trap gas (aspect ratio greater than 7.2). This aspect ratio value is in a reasonable agreement with Bankoff [12] and Lorenz [13] as seen in Fig. 4. It is worth mentioning that the capillary rise equation is not recommended for cavity design because it depends on other forces such as viscous force that depend on liquid velocity and viscosity. It was used here only for rough validation. In conclusion, because Bankoff and Lorenz gas entrapment criterion ($\theta > 2\beta$) works for both hydrophilic and hydrophobic surfaces, the current authors recommend it for the design of surface cavities as a general criterion. Also, the authors recommend that the static contact angle (worst case scenario) should be used with the gas entrapment criteria rather than dynamic contact angles.

In conclusion, the review of the existing gas entrapment criteria indicated that three researchers (Winterton [15], Cornwell [16], Wang and Dhir [17] reported that wetting liquids (θ less than 90) cannot trap gas in conical cavities. On the contrary, Bankoff [12], Lorenz [13] and Tong et al. [14] reported the opposite provided that the contact angle is greater than the cavity cone angle. If the first group of researchers are correct (wetting liquids cannot trap gas), the incipient superheat will be significantly high. In literature, one can see that several experimental studies with moderately wetting liquids reported low wall superheat at boiling incipience which indicates that there is possibility of gas entrapment in the surface cavities. The authors of the present paper believe that the difference between the criteria given by Bankoff [12] and Winterton [15] arises from differences in the definition of the contact angle. In the Bankoff criterion, the liquid front (see Fig. 3a) was assumed to propagate on one of the side walls of the cavity and trapping occurs when it touches the opposite side wall. In other words, trapping was deemed to happen immediately before the liquid–vapour interface touches the opposite wall, i.e. before it reaches mechanical equilibrium. This is the classical definition of the advancing contact angle (wettability angle). In the Winterton criterion, entrapment was deemed when the liquid–vapour interface was at mechanical equilibrium. When the liquid at the wall is sub-cooled (the boiling surface temperature is significantly below saturation), the vapour pressure is very small and thus mechanical equilibrium requires that the liquid–vapour interface be concave in the liquid side ($P_L > P_v$). It means that even if the liquid is wetting, the angle formed after equilibrium will be greater than $90^0$. This angle is not the wettability angle but it is the angle formed due to the pressure difference across the interface. In other words, Bankoff [12] and Winterton [15] were referring to two different angles.

### *Nucleation site stability*

Nucleation site stability is another factor that should be considered in the design of boiling heat transfer surfaces, especially with purposely made artificial nucleation sites. Once activated, the cavity should remain active with insignificant variations in surface temperature. In some cases, the active cavity becomes inactive for a while and thus the local surface temperature increases rapidly resulting in large spikes in the surface temperature. Qi and Klausner [21] investigated heterogeneous nucleation from artificial cylindrical cavities manufactured on a silicon substrate with diameter ranging from 8 to 60 μm and depth 45 μm. They conducted the test using water (contact angle 21) and ethanol (contact angle nearly zero). It was observed that cavities were not stable and bubble nucleation was intermittent, i.e. cavities become inactive for some minutes before starting again. They attributed this to enhancement in convection currents induced by bubble ebullition, which results in a thinner boundary layer, and thus suppress nucleation at some locations. The mechanism of instability was first introduced by Marto and Rohsenow [22] to explain the large fluctuations in surface temperature during boiling of liquid metals (highly wetting liquids). When the bubble departs the nucleation site, it leaves vapour residuals at the cavity mouth. Due to the drop-in surface temperature during the ebullition cycle, part of the vapour residuals may condense and penetrate the cavity. When the liquid gains heat from the condensed vapour and from the wall, its temperature increases and thus condensation stops. The distance at which condensation stops is called the maximum penetration depth ($x^*$). If the cavity depth was smaller than the maximum penetration depth, the embryo will collapse, and the cavity will be flooded and therefore high wall superheat will be required to start the cycle again. Although this mechanism was suggested based on boiling of liquid metals, Kosky [23] studied experimentally boiling of deionized water in glass capillary tube with an inner diameter 0.1 mm and observed the same phenomena. The measured maximum penetration distance after bubble departure ranged from 50 to 500 μm.

Marto and Rohsenow [22] conducted a theoretical study and solved the transient heat conduction equation and the equation of motion of the liquid–vapour interface inside a cylindrical cavity for contact angle $\theta < 90^0$. They gave the following criterion for the critical cavity depth above which the cavity will be stable:

$$x^* > \frac{4}{\pi}\left(\frac{T_{sat}^2}{\rho_v^3 h_{fg}^3}\right)\left(\frac{2\sigma cos\theta}{r_c}\right)^2 (1+0.5\varepsilon)^2 K^2 \left[\frac{\sqrt{\rho_w c_w k_w}\sqrt{\rho_L c_{pl} k_L}}{20q(1+sin\theta)}\right], K = \frac{aq}{k_w\left(q\sqrt{f/\alpha_w}\right)^b} \quad (1)$$

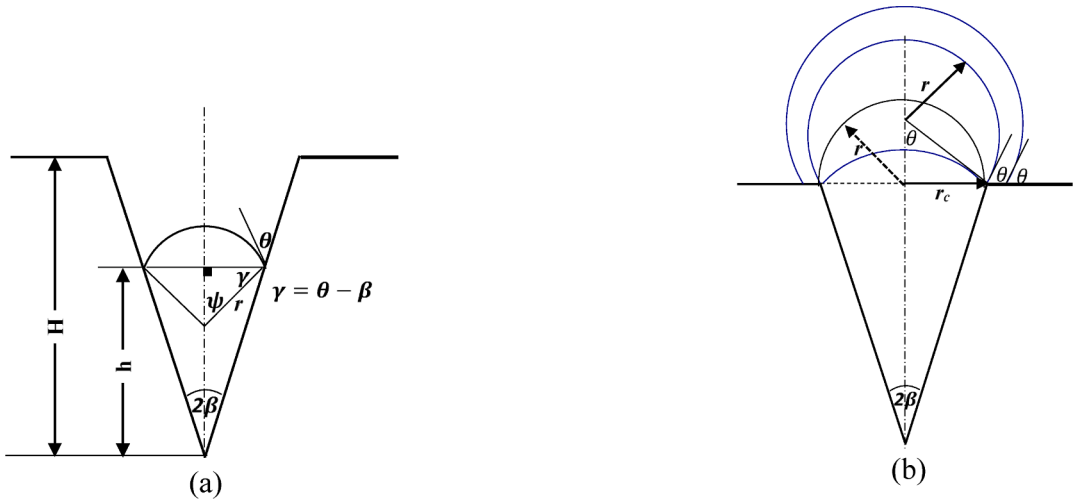


**Fig. 6.** Growth of bubble embryo (a) inside the conical cavity and (b) at the cavity mouth.

In the above equation, Marto and Rohsenow recommended a value of 0.3 for $\varepsilon$, which is an empirical parameter used to approximate the wall temperature rise during the waiting period, $f$ is the bubble generation frequency. The constants $a$ and $b$ are empirical and depend on the type of material and rms roughness. They gave values of 41.2 and 0.706 for aluminum with roughness rms = 13 μm and 5.865 and 0.63 for stainless steel with roughness rms = 19 μm. These empirical constants were based on the experimental measurements of the transient local surface temperature during pool boiling of water conducted by Hsu and Schmidt [24]. It is worth mentioning that the above equation was based on many assumptions and can be used to give an idea about the stability of cavities designed based on the entrapment criterion given by Bankoff [12]. The evaluation is conducted here for a bubble generation frequency value of 30 Hz, a heat flux value of 35 kW/m$^2$ (about 6 K wall superheat), water and FC-72. The following can be concluded from Eq. (1): (i) for the same fluid and material, the maximum penetration distance decreases as the cavity mouth radius increases for a fixed value of contact angle, i.e. improved stability. In fact, this agrees with the capillary rise discussed above ($h_c = 2\sigma\cos\theta/\rho_l g r_P$), which indicates that the height decreases as the radius increases, (ii) for a fixed material and contact angle, the maximum penetration depth of FC-72 is much less than that of water, i.e. cavities are more stable with FC-72 compared to water. (iii) for the same fluid and fixed contact angle, the penetration depth in case of aluminum is much smaller than that of stainless steel, i.e. stability is better for metals with larger $\sqrt{\rho_w c_w k_w}$. For water, if the contact angle was assumed to be $60^0$ and the cavity radius is 10 μm, the minimum cavity depth from Fig. 4 will be 11.5 μm for Bankoff criterion. Based on Eq. (1), for $\theta = 60^0$ and cavity radius of 10 μm, the predicted penetration depth is about 0.2 μm, which is much smaller than the designed cavity depth (11.5 μm). For FC-72 with assumed contact angle $\theta = 10^0$ and cavity radius 10 μm, the required minimum cavity depth from Fig. 4 is 114 μm while the liquid penetration depth based on Eq. (1) is less than 0.05 μm. Accordingly, it can be concluded that cavities designed based on Bankoff entrapment criteria are stable regardless of cavity diameter, type of fluid and material properties.

*Incipient superheat*

Prediction models of the incipient superheat start usually with mechanical and thermodynamic equilibrium for a spherical bubble embryo (Young-Laplace equation combined with Clausius-Clapeyron equation). This results in Eq. (2) below, which predicts the wall superheat in terms of fluid properties and embryo radius.

$$\Delta T_{sup} = (T_w - T_{sat}) = \frac{2\sigma T_{sat} v_{fg}}{r_e^* h_{fg}} \tag{2}$$

The only unknown in the above equation is the radius of bubble embryo at the onset of nucleation, which is called the critical radius ($r_e^*$). The design of a high-performance boiling surface requires cavities that can be activated at low wall superheat. The different approaches of predicting the incipient superheat are summarized below.

*Phase stability-based models*

From the fundamentals of thermodynamics, it is known that phase transition occurs under non-equilibrium conditions, e.g. boiling occurs when the liquid temperature exceeds the equilibrium saturation temperature (superheated liquid). This non-equilibrium state of a liquid is usually called "metastable state". The condition required for mechanical stability in a metastable state is given as:

$$\left(\frac{\partial P}{\partial v}\right)_T \leq 0 \tag{3}$$

Boiling starts when there is a deviation from the metastable state, i.e. under unstable conditions. The above criterion in Eq. (3) can be applied for the stability of a growing vapour nucleus (thermodynamic system) assuming that the pressure is the capillary pressure, $P_c = 2\sigma/r$ and the surface tension is constant at isothermal conditions. The condition required for stability is that the slope of the $P$-$v$ curve at a fixed temperature must be negative. The positive slope is not realistic (unstable state) because it means that the volume increases as the pressure increases – something impossible. Thus, Eq. (3) can be re-written as:

$$\left(\frac{\partial P_c}{\partial v}\right)_T \leq 0 \text{ or } \left(\frac{\partial (1/r)}{\partial v}\right)_T \leq 0 \tag{4}$$

The nucleation problem can now be understood from the relation between embryo curvature ($1/r$) and volume. Note that from Eq. (2), the wall superheat is proportional to $1/r$. This criterion will be applied in this section for a bubble embryo in a conical cavity with the geometry defined in Fig. 6. When the bubble embryo is inside the cavity (Fig. 6a), the volume of the vapour can be calculated from trigonometric relations as a function of embryo radius ($r$), contact angle ($\theta$) and cavity cone half-angle (β). In this case, the total volume equals the sum of the volume of a spherical bubble cap and the volume of a cone as given by Eq. (5) below.

$$V = \frac{\pi r^3}{3}(1-\cos\psi)^2(2+\cos\psi) + \frac{\pi r^3}{3}\frac{sin^3\psi}{\tan\beta}, \psi = 90 - (\theta - \beta) \tag{5}$$

When the embryo grows and reaches the cavity mouth as shown in

Fig. 6b, the liquid–vapour interface rotates around the cavity edge until the wettability contact angle is reached, i.e. transition from the cavity wall to the main surface wall. Similar equations, as Eq. (5), can be obtained in a similar manner when the embryo sits on the cavity mouth. On doing so, the curvature ($1/r$) can be plotted versus volume for a fixed cavity cone angle ($2\beta$) of $20^0$, cavity radius 5 μm and different values of contact angle ($\theta$). Fig. 7 depicts the curvature versus volume for $h/H = 0.4$ (see Fig. 6a for nomenclature), $\theta = 30^0$, $\theta = 60^0$, $\theta = 90^0$ and $\theta = 110^0$ as an example. In other words, the cavity is partially filled with gas and the rest is liquid. The calculated cavity depth is 28.4 μm and aspect ratio is 2.84. For contact angles $\leq 90^0$, the figure indicates that: (i) the curvature is positive (convex interface) and it decreases with increasing volume when the embryo grows inside the cavity, i.e. the slope is negative and the liquid–vapour interface is stable. (ii) when the three-phase contact line (TPL) reaches the cavity edge, the curvature increases with increasing volume and reaches its maximum value when $r = r_c$, i.e. positive slope means unrealistic and unstable liquid–vapour interface. (iii) when the radius of curvature exceeds the cavity mouth radius, the curvature decreases again with increasing volume, i.e. the slope becomes negative again and the embryo can continue to grow up to the departure size. In the non-wetting case (contact angle $110^0$), the curvature inside the cavity is negative (concave interface), as seen in Fig. 7, and the curvature increases as the volume increases (unrealistic unstable case). After that the curvature changes from negative to positive at the cavity mouth but it remains unstable, i.e. the curvature increases as the volume increases. When the curvature reaches its maximum value at the cavity mouth radius, the interface becomes stable and the bubble continues its growth up to departure. In other words, in hydrophobic cases, bubble growth starts from the cavity mouth.

Some researchers [13,14,17,25] adopted the phase-stability theory to predict the critical embryo radius required for the prediction of the incipient superheat using Eq. (2) mentioned above. Griffith and Wallis [25] reported that, for a wide range of contact angle ($\beta < \theta < 90$), nucleation starts when the curvature reaches its maximum value (see Fig. 6 for $\theta = 90^0$), which occurs at the cavity mouth ($r_e^* = r_c$). It is worth noting that, based on our calculations, this criterion is valid for a wide range of contact angles only if the location of the TPL is very near to the cavity mouth ($h/H \approx 0.8 - 0.9$), i.e. the cavity traps large amount of gas. For example, when $h/H = 0.4$, the above calculations indicates that the criterion by Griffith and Wallis is valid for $\theta > 76^0$ (narrow range of wetting liquids). When $h/H = 0.8$, their criterion is valid for $\theta > 47^0$ (wide range of wetting liquids). To evaluate this criterion, they measured the incipient superheat using water and a single artificial cavity of diameter 68.6 μm fabricated on a copper surface. It was found that the measured superheat was 20 K while Eq. (2) predicts 3 K. They attributed this disagreement to the use of mean wall superheat rather than the local superheat, i.e. wall superheat at the cavity is expected to be much lower. Wang and Dhir [17] conducted thermodynamic analysis and determined the conditions at which the interface becomes unstable. They reached the same conclusion as Griffith and Wallis for $\theta \leq 90$, i.e. the critical embryo radius equals the cavity mouth radius at boiling incipience. For $\theta > 90$, the critical embryo radius was found to depend on the contact angle, $r_e^* = r_c/\sin\theta$.

Lorenz [13] reported that highly wetting liquids can penetrate the cavity and thus the critical embryo radius can be smaller than the cavity mouth radius. In other words, the embryo curvature can reach its maximum value inside the cavity as seen in Fig. 7 for $\theta = 30^0$. Thus, he proposed a simple model that relates the bubble embryo radius to the cavity geometry and contact angle, see Fig. 8 that shows the model schematic. It was assumed that a liquid with a flat interface advances with contact angle ($\theta$) towards the cavity and traps an initial volume of gas (Fig. 8a). The calculated volume in Fig. 8a equals the volume of a truncated cone. After the interface recedes in the cavity, the interface changes from flat to curved shape with radius of curvature ($r_e$), Fig. 8b. The volume in this case will be the same as the one calculated by Eq. (5), i.e. volume of cone plus a spherical cap. Lorenz calculated the change in volume when the interface changes from flat into curved shape and obtained the ratio of the embryo radius to the cavity mouth radius as given by Eq. (6) below which is plotted in Fig. 9. Based on that, if $f < 1$ (embryo radius is smaller than the cavity mouth radius), the critical embryo radius will be given as $r_e^* = fr_c$. If the opposite occurs, the critical embryo radius will be the cavity mouth radius ($r_e^* = r_c$).

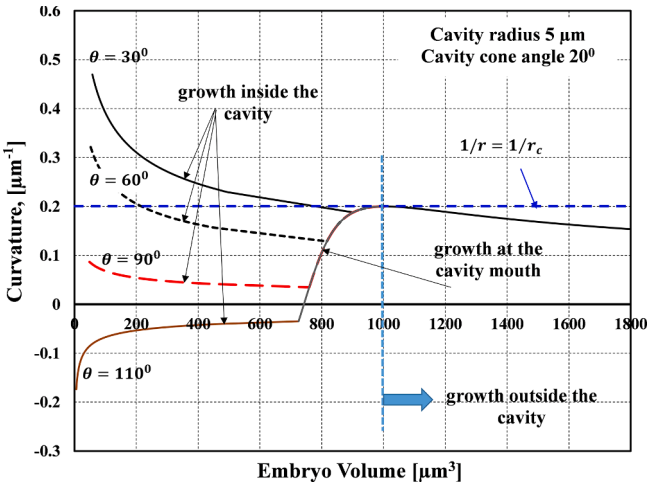


**Fig. 7.** Curvature versus embryo volume during bubble nucleation from a conical cavity assuming that the cavity traps small quantity of gas.


**Fig. 8.** Schematic drawing for the nucleation model by Lorenz [13], (a) advancing liquid front with a flat interface, (b) interface curvature after the embryo stabilizes inside the cavity.

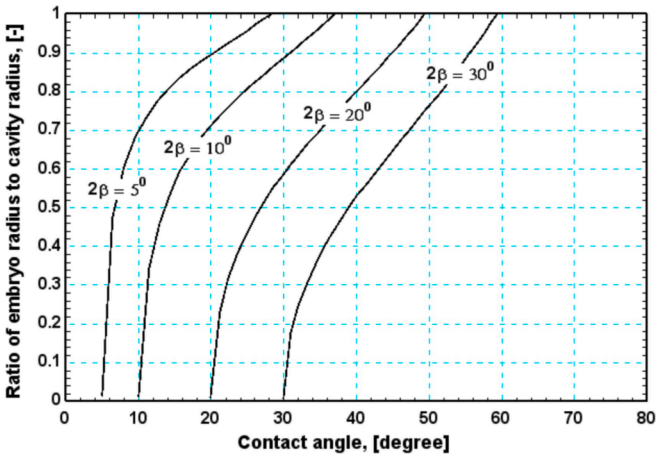


**Fig. 9.** Effect of cavity cone angle and contact angle on the critical embryo radius predicted using Lorenz [13].

$$f = \frac{r_e}{r_c} = \left[ \frac{\frac{\sin(\theta-2\beta)\tan^3\psi(\tan\gamma\cot\psi-1)^2}{\sin\beta\cos\gamma(\tan^2\psi-\tan^2\gamma)^{3/2}}}{\left[\frac{\cos^3(\theta-\beta)}{\tan\beta} + (1-\sin(\theta-\beta))^2(2+\sin(\theta-\beta))\right]} \right]^{1/3}, \psi = 90-\beta, \gamma = 90-(\theta-\beta) \quad (6)$$

Tong et al. [14] modified the Lorenz [13] model by taking the effect of contact angle hysteresis into account, i.e. the dynamic contact angle was used in Eq. (6) instead of the static contact angle. The modified model is plotted in Fig. 10a and 10b for cavity cone angle $5^0$ – $30^0$. The original and modified models indicate that the contact angle (static or dynamic) should be greater than the cavity cone angle, which agrees with Bankoff entrapment criterion. When the contact angle is less than the cone angle, the solution of Eq. (6) does not exist. Additionally, Fig. 9 indicates that, for a fixed cavity cone angle, there is a certain contact angle value above which the ratio becomes greater than 1 (bubble embryo radius exceeds the cavity mouth radius and thus $r_e^* = r_c$). For example, for a cone angle of $5^0$, the ratio exceeds 1 for contact angle greater than $28^0$. For contact angle below $28^0$, the critical embryo radius should be $r_e^* = fr_c$, where $f$ is a fraction <1, which depends on the contact angle. Fig. 10a demonstrates that for highly wetting liquids with $\theta = 5^0$ when the contact angle hysteresis was taken into consideration, the ratio $(r_e/r_c)$ is always less than 1 while for $\theta = 40^0$ in Fig. 10b (moderately wetting liquids), the ratio is always above 1 for cavity cone angle below $20^0$ regardless of the dynamic contact angle.

The model by Tong et al., [14] depends on the dynamic contact angle which is a complex parameter that depends on the velocity of the three-phase contact line. Thus, the Lorenz model will be used in this section to predict the boiling incipience superheat and quantify the effect of fluid properties and wettability. Fig. 11 shows the effect of contact angle on the predicted wall superheat for FC-72 and cavities with cone angle $5^0$ (Fig. 11a) and $40^0$ (Fig. 11b). It is worth noting that FC-72 is a highly wetting liquid and the effect of contact angle in Fig. 11 may be corresponding to changing the wettability by surface coating. Also, the figure includes prediction using Eq. (2) with $r_e^* = r_c$ as recommended by Griffith and Wallis [25] and Wang and Dhir [17]. The two extreme cases in Fig. 11a and 11b (small and large cone angles) can represent a surface with a range of deep cavities (cone angle $5^0$) and shallow cavities (cone angle $40^0$). Small cone angle cavities could exist when the surface roughness profile exhibits large waviness frequency (see Fig. 5) while large cone angle could exist when the frequency of the waviness is low.

Fig. 11a indicates that, the effect of contact angle is only limited to contact angles in the range 5 – $28^0$ for cavity cone angle $5^0$ while this range in Fig. 11b is $40^0$ – $68^0$ for cavity cone angle $40^0$. For contact

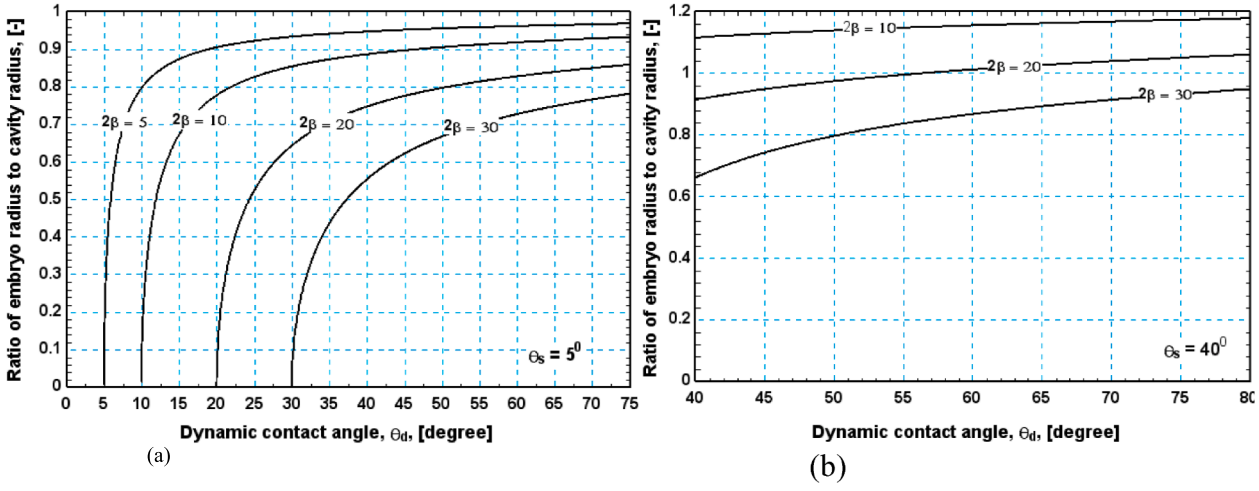


**Fig. 10.** Effect of cavity cone angle and contact angle on the critical embryo radius predicted using Tong et al. [14] for (a) highly wetting fluid, (b) moderately wetting fluid.

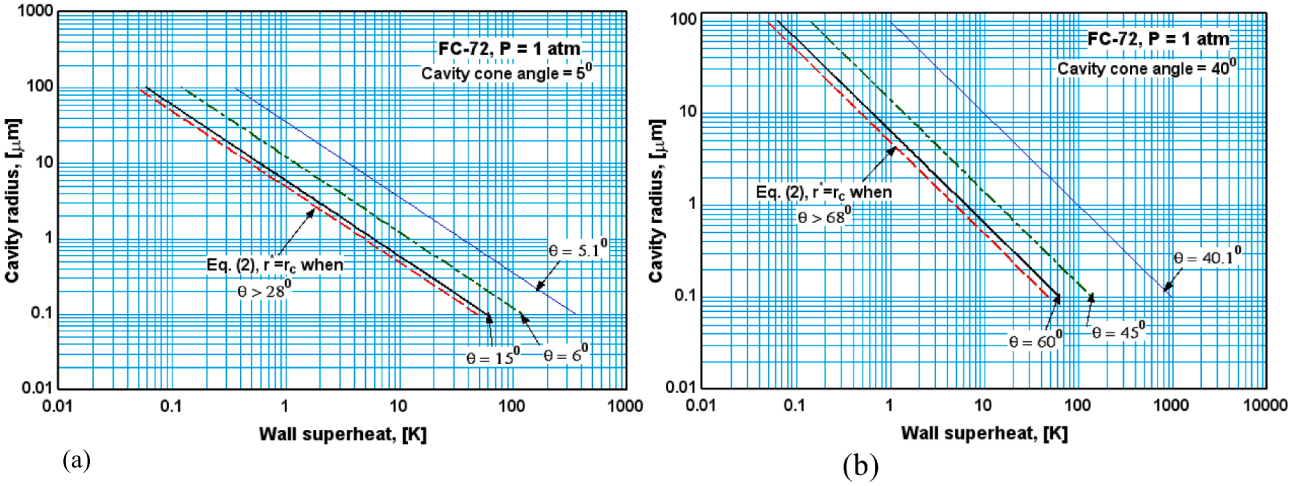


**Fig. 11.** Effect of contact angle on boiling incipience wall superheat predicted using Lorenz [13] for (a) cavity with cone angle = $5^0$ and (b) cavity with cone angle = $40^0$.

angles above $28^0$ and $68^0$, there is no wettability effect and the Lorenz model predicts values similar to Eq. (2) with $r_e^* = r_c$. In other words, the cavity mouth radius will be the only geometrical parameter required to predict the incipience superheat. Fig. 11 indicates also that ignoring the effect of wettability and using Eq. (2) simply with $r_e^* = r_c$ can result in significant under-prediction. For example, at cavity mouth radius of 1.1 μm in Fig. 11a, Eq. (2) with $r_e^* = r_c$ predicts a superheat value of 4.36 K. For FC-72 with contact angles $15^0$, $6^0$ and $5.1^0$, Lorenz model predicts 5.31 K (21.7 % higher), 10.9 K (150.7 % higher) and 31.9 K (632 % higher). For surfaces with nanostructure, the incipient superheat is extremely large and there is no possible nucleation when the cavities are nearly flooded (contact angle slightly larger than the cavity cone angle), e.g. for $r_c = 0.1\mu m$, $\Delta T_{sup} > 300K$ in Fig. 11a and $\Delta T_{sup} > 900K$ in Fig. 11b. When the contact angle is extremely larger than the cavity cone angle, the superheat for $r_c = 0.1\mu m$ (nanostructure) is still large (about 50 K). It is obvious from Fig. 11 that, to keep the superheat below 10 K and if the surface design will be based on the worst-case scenario (contact angle slightly larger than the cavity cone angle, $\theta = 5.1^0$ in Fig. 11a), the surface microstructure should include cavities with radius greater than 3.5 μm. Thus, the surface specifications for FC-72 with small cavity cone angle is that the minimum cavity mouth diameter should be 7 μm and the minimum cavity depth should be 80 μm. Additionally, the worst-case scenario in Fig. 11b (contact angle slightly greater than the cone angle, $\theta = 40.1^0$) requires that the surface should have cavities with radius above 10 μm to keep the wall superheat below 10 K. This gives cavities with diameter 20 μm and depth 28 μm. It is worth mentioning that the contact angle with values slightly larger than the cavity cone angle ($\theta = 5.1^0$ and $40.1^0$) were used to simulate the flooded cavities bearing in mind that the contact angle should be greater than the cavity cone angle (there is no solution for the model (Eq. (6)) when the two angles are equal).

Fig. 12, compares water, which is a moderately wetting liquid with FC-72 and HFE-7100, which are highly wetting liquids. The surface was assumed to be the same as if the three fluids were tested on the same surface, e.g. copper surface. For water, a contact angle of $60^0$ was assumed with copper (commonly measured in literature), while the assumed value for FC-72 and HFE-7100 was $10^0$ (highly-wetting). The cavity cone angle was assumed fixed with $5^0$ (simulating a surface with high roughness wave frequency). The figure includes also a case for water with contact angle $10^0$ for the sake of comparison. According to the Bankoff criterion, it is expected that cavities can trap more gas with water compared to FC-72 and HFE-7100 because the water contact angle is much greater than the cavity cone angle. Thus, based on the gas entrapment criterion alone, the wall superheat is expected to be much lower for water. However, Fig. 12 indicates that the wall superheat for water can be up to 376 % higher than that for FC-72, for the same cavity radius. The wall superheat of HFE-7100 can be up to 72 % larger than that of FC-72 although they have the same wettability. This means that fluid thermophysical properties can have a much greater effect on the incipient wall superheat compared to the effect of wettability. The effect of fluid thermophysical properties can be understood from Eq. (2), which can be written in the form: $\Delta T_{sup} = 2\sigma/rs$, where $s$ is the slope of the vapour-pressure curve: $s = h_{fg}/v_{fg}T_{sat}$. It is worth noting that the slope of the vapour pressure curve ($s$) at atmospheric pressure is 3.58 kPa/K for water, 3.36 kPa/K for FC-72 and 3.24 kPa/K for HFE-7100. This difference in slope is not significant to cause the big difference in the predicted wall superheat. Accordingly, the most important fluid property that affect the incipient wall superheat is surface tension because the difference in slope for most fluids of interest is small at low pressures. Compared to FC-72 and HFE-7100, the surface tension of water is 7.5 and 4.3 times larger. It is worth noting also that the surface tension of HFE-7100 is 1.7 times larger than that of FC-72. As a rule of thumb, based on the phase-stability model of Lorenz [13], as the surface tension increases the incipient wall superheat increases for fluids having the same slope of vapour pressure curve and for the same cavity radius and cavity cone angle.

*Superheated boundary layer-based models*

In the above discussion, the wall superheat at boiling incipience can be predicted using Eq. (2) after considering the effect of wettability on the critical embryo radius as discussed above. Hsu [3] argued that Eq. (2) predicts wall superheat that approaches zero when the cavity mouth radius approaches infinity – something which is not practically feasible. Additionally, Hsu reported that, in engineering surfaces, there is a range of cavity sizes that can be activated for a fixed wall superheat value rather than one single size as predicted by Eq. (2). Accordingly, he proposed a nucleation criterion which depends on the characteristics of the thermal boundary layer at the heated wall as seen in Fig. 13. It was assumed that there is a bubble embryo (truncated sphere) sitting on the cavity mouth and nucleation occurs (the bubble grows until departure) when the liquid temperature in the thermal boundary layer is at least equal to the vapour bubble temperature. The liquid temperature was obtained from the solution of the transient one-dimensional heat conduction equation and the vapour bubble temperature was obtained from the Clausius-Clapeyron equation. On doing so, Hsu obtained a quadratic equation that predicts the range of active nucleation sites as given by Eq. (7) below.

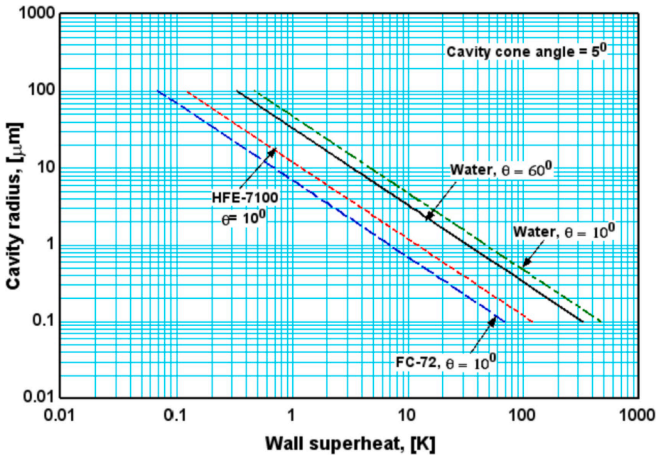


**Fig. 12.** Effect of fluid type on boiling incipience wall superheat predicted using Lorenz [13] for cavity with cone angle = $5^0$.

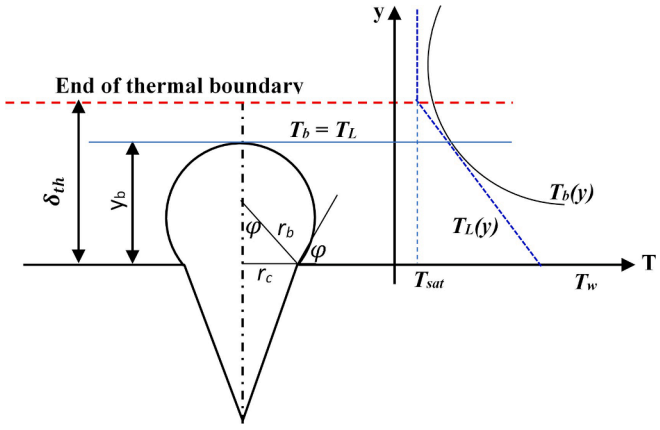


**Fig. 13.** Schematic drawing for the thermal boundary layer nucleation model suggested by Hsu [3]

$$r_c(max,min) = \frac{\delta_{th}}{2}\frac{\sin\varphi\Delta T_{sup}}{(1+cos\varphi)(\Delta T_{sup}+\Delta T_{sub})}\left[1 \pm \sqrt{1-\frac{8(1+cos\varphi)\sigma T_{sat}(\Delta T_{sup}+\Delta T_{sub})}{\delta_{th}\rho_v h_{fg}\Delta T_{sup}^2}}\right] \quad (7)$$

$$y_b = (1+\cos\varphi)r_b r_c = r_b sin\varphi$$

In Eq. (7), the angle φ is not the wettability contact angle. It is the angle that the embryo bubble makes with the surface when the bubble temperature equals the liquid temperature (shape angle), measured from the liquid side as seen in Fig. 13. It depends on the model assumption, i.e. $\varphi = 90^0$ if hemispherical bubble was assumed. In Eq. (7), $y_b$ is the bubble height measured from the heating surface at which the liquid and bubble temperature are equal. It is worth mentioning that some researchers, see for example Dahariya and Betz [26], Thiagarajan et al. [27] and Yu and Cheng [28], used the static contact angle in the above equation, which is not what is required in the model. In conclusion, all thermal boundary layer models did not take the effect of wettability into account. For the effect of wettability, the models discussed in section 2.3.2 should be adopted for the prediction of the critical embryo radius required for nucleation. In his analysis, Hsu assumed that the liquid temperature equals the bubble temperature when $y_b = 2r_c$, which according to the above relations in Eq. (7) gives $\varphi = 53.1^0$. Han and Griffith [29] solved the transient 1D heat conduction equation assuming that the liquid is a solid slab and with the assumption of linear temperature profile near the wall. They treated the bubble in the thermal layer as a solid insulated sphere and from the potential flow theory, they found that the equality between bubble and liquid temperature occurs when $y_b = 1.5r_c$. This is corresponding to an angle $\varphi = 67.4^0$. Bergles and Rohsenow [30] recommended that the equality between the bubble and liquid temperature occurs when $y_b = r_c$, which is corresponding to an angle $\varphi = 90^0$. Kandlikar et al. [31] conducted numerical analysis for the flow around a nucleating bubble in mini-channels and found that the equality of temperature occurs when $y_b = 1.1r_b$, which corresponds to an angle $\varphi = 84.3^0$.

These models are compared in Fig. 14 for saturated pool boiling of water at atmospheric pressure. It is worth mentioning that the thermal boundary layer thickness was calculated from the natural convection heat transfer coefficient and the liquid thermal conductivity, $\delta_{th} = k_l/h_{nc}$. For water, the calculated boundary layer thickness at 5 K temperature difference is 0.608 mm. For a fixed superheat value of 10 K, the predicted cavity size range from these models is as follows: 4.16 – 513.5 μm using the Kandlikar model, 2.65 – 283.1 μm using the Hsu model, 3.3 – 568.6 μm using the Bergles and Rohsenow, 3.06 – 377.7 μm using the Han and Griffith model and the value predicted using Eq. (2) with $r_e^* = r_c$ is 3.29 μm. This comparison indicates that there is some difference in the predicted maximum cavity radius while there is reasonable agreement on the predicted minimum cavity radius. It is interesting to note that Eq. (2), which is very simple, agrees very well with the minimum cavity radius predicted using the thermal boundary layer models. Because the differences between the above models are small, the Hsu model was selected to examine the effect of subcooling (Fig. 15), system pressure (Fig. 16) and fluid type (Fig. 17). Fig. 15 indicates that for the same wall superheat, the maximum cavity size decreases with increasing the degree of subcooling, i.e. the range of active nucleation sites decreases. Fig. 16 indicates that the minimum cavity size decreases with increasing system pressure. In other words, the maximum cavity size is affected by the degree of subcooling due to the decrease in thermal boundary layer thickness with increasing degree of subcooling. The minimum cavity radius, for a fixed degree of subcooling, depends on fluid properties and thus it decreases with increasing system pressure due to the reduction in surface tension (22.6 %) and the significant increase in the slope of the vapour-pressure curve (561 %) when the pressure increased from 0.5 to 5 bar. Fig. 17 compares the range of cavity size for water, FC-72 and HFE-7100 at atmospheric pressure and 5 K subcooling. It indicates that for wall superheat value of 10 K, the range of active nucleation sites will be 5.5 – 126 μm, 0.7 – 108 μm, 0.4 – 79 μm for water, HFE-7100 and FC-72, respectively. Based on the minimum cavity size at the same superheat, water requires cavities with radius which is about 14 times larger compared to FC-72. For the same cavity size (1 μm), the wall superheat

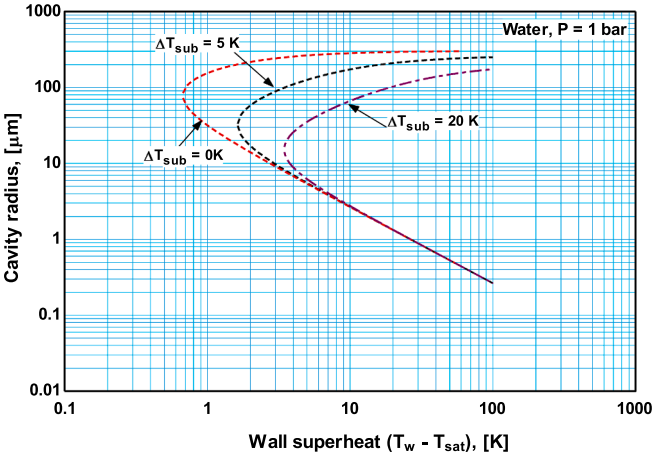


**Fig. 15.** Effect of subcooling on the size range of cavities predicted using Hsu [3] model.

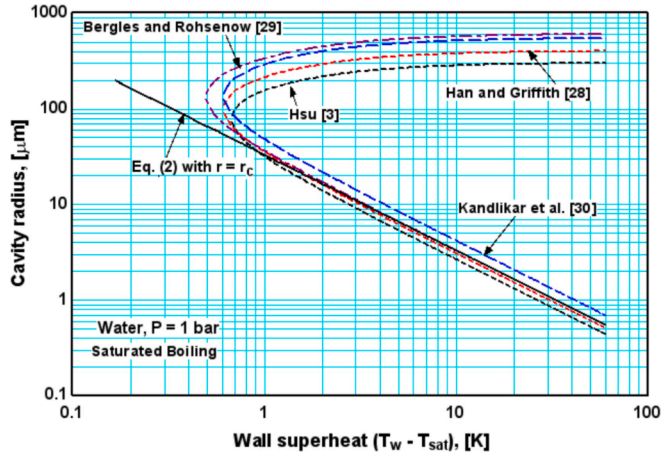


**Fig. 14.** Comparison between nucleation models for water at atmospheric pressure.

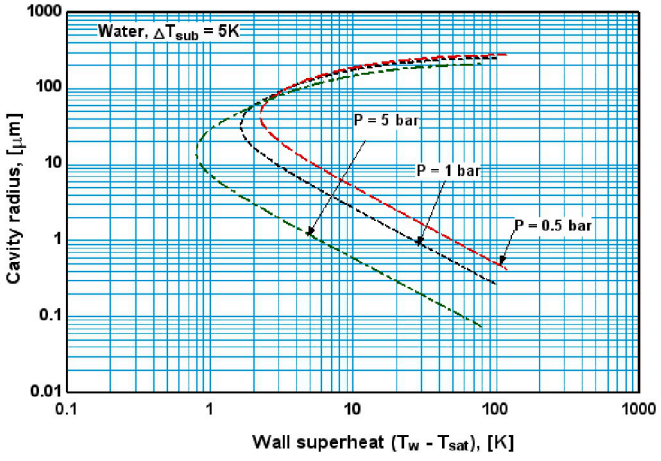


**Fig. 16.** Effect of system pressure on the range of active nucleation sites predicted using Hsu [3] model.

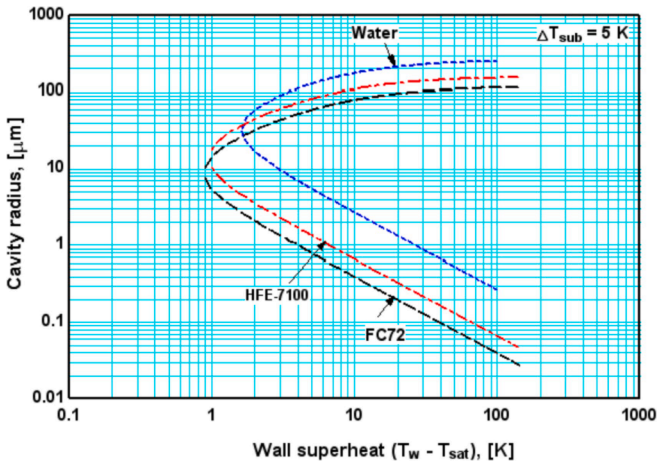


**Fig. 17.** Effect of fluid on the size range of nucleation sites predicted using Hsu [3] model.

required at boiling incipience is much higher for water compared to FC-72 and HFE-7100. Based on the maximum cavity radius, the opposite occurs, i.e. wall superheat of water is much lower than that of FC-72 and HFE-7100. In other words, water may perform better on micro-finned surfaces, rather than smaller surface structure preferred by more highly wetting fluids like refrigerants.

In conclusion, the boiling incipience superheat can be predicted either using the phase stability-based models (wettability-based models) or the thermal boundary layer-based models. In the wettability-based models [13,14], the critical embryo radius was given as a function of cavity mouth radius, wettability and fluid properties. In the thermal boundary layer-based models [3,29 –31], the critical embryo radius was given as a function of the cavity mouth radius, the bubble shape angle, the boundary layer thickness and fluid properties. All thermal boundary layer-based models [3,29 –31] conclude that the cavity mouth diameter is the only geometrical parameter needed for the design of surface cavities regardless of wettability. On the contrary, the wettability-based models by Lorenz [13] and its modified version by Tong et al. [14] recommend that cavity depth and cavity mouth diameter are important for the surface design especially for highly wetting liquids. These models [13,14] predict that for a fixed cavity cone angle, the incipient superheat decreases as the contact angle increases up to a certain contact angle value above which the effect of wettability diminishes. They could explain the very high superheat encountered with highly wetting liquids – something which the other thermal boundary layer-based models could not explain. Also, they predict that for highly wetting liquids, the cavity aspect ratio should be greater than 10 while it should be 2 – 3 for moderately wetting liquids. Additionally, the models [13,14] indicated that for a fixed cavity size and fluids with the same slope of vapour-pressure curve, the incipience superheat increases as surface tension increases. However, some experimental studies tested different fluids on the same substrate material and the effect of surface tension did not follow the conclusion from Lorenz [13] model, as will be discussed below in the next section. The wettability-based models cannot predict the effect of liquid bulk temperature (degree of subcooling) while the thermal boundary layer-based models predict that the range of active nucleation sites decreases with increasing degree of liquid subcooling.

*On the validation of boiling incipience models*

Although the above theories have been developed some time ago, there is no study with the objective of validating these theories. This could be due to the difficulty in the fabrication of conical cavities and the measurement of the local superheat underneath each cavity. In this paper, the incipient superheat is detected from the boiling curve from some of the relevant past studies, in order to shed some light on the validation of the above theories. Surtaev et al. [32] investigated saturated boiling of water and ethanol on sapphire substrate with transparent heating. The roughness of the boiling surface was less than 1 nm (based on manufacturer data sheet as they did not measure it) and the static contact angle was $60^0$ for water and $10^0$ for ethanol. With this surface finish, it was expected that the incipience superheat approaches the value in homogeneous nucleation, e.g. 213.3 K for water. However, the boiling curve for water indicated that boiling started at wall superheat of 22.3 K with 4 K excursion while for ethanol the incipient superheat and the excursion were 47.4 K and 11.2 K, respectively. This temperature excursion could be an indication of the gas entrapment at the beginning (the first embryo cycle). Additionally, both fluids exhibited boiling incipience hysteresis but the slope of the water boiling curve was much larger compared to ethanol, i.e. better heat transfer rate. It is interesting to note that the surface tension of water is about 3.3 times greater than that of ethanol. As discussed above (see section 2.3.1), the incipient wall superheat increases as surface tension increases for a fixed cavity size. Thus, it might be expected that the wall superheat at boiling incipience should be lower for ethanol, which was not the case. This behaviour may lead to the conclusion that cavities that were activated with water are different from those that were activated with ethanol bearing in mind that the boiling surface is the same but it may have a wide range of random cavity sizes. To verify this conclusion, the cavity size can be estimated by back calculations using the measured contact angle and wall superheat. From Eq. (2), the predicted critical embryo radius for water and ethanol are 1.5 μm and 0.19 μm, respectively. Using the Lorenz [13] model and the measured contact angle for each fluid, the cavity cone angle and cavity mouth radius can be predicted. For ethanol with contact angle $10^0$ and 47.4 K superheat, the model predicted that the effective embryo radius (0.19 μm) exists always inside the cavity and there is a range of cavity sizes (all cavities with cone angle less than $10^0$) that can satisfy the superheat value (47.4 K). The cavity mouth radius ranged from 0.3 to 0.7 μm. On the contrary, for water with contact angle $60^0$ and 22.4 K superheat, the model predicted that the effective embryo radius (1.5 μm) can satisfy the superheat value of 22.4 K over a wider range of cavity sizes. This range include cavity sizes with possible nucleation at the cavity mouth (all cavities with cone angles $\langle 30^0$) and another range of cavity sizes with possible nucleation from inside the cavities (all cavities with cone angle $> 30^0$). The cavity mouth radius was in the range 1.5 – 5 μm. For ethanol, the predicted smallest cavity depth and aspect ratio at incipience are 5.7 μm and 8.6, respectively. For water, the minimum cavity depth and aspect ratio at incipience are 5.6 μm and 1.86, respectively. Note that, the cavity diameter is not the same because the cavity cone angle is different for each fluid. These values are not matching the surface characteristics of the smooth substrate in the study by [32]. However, it does not mean that the models are not accurate because, in practice, surface analysis is usually conducted for a tiny area of the surface. Besides, the authors did not characterize the surface. It is worth noting that few debris on the surface can act as nucleation sites. It is interesting to note that the Lorenz model predicted a range of active cavities for a fixed superheat value – something similar to the Hsu model. Evaluating the Hsu model indicates that the range of active cavities for water at 22.3 K is 1.19 – 294 μm and for ethanol at 47.4 K is 0.15 – 106 μm. The maximum cavity radius is impossible to exist on the investigated transparent substrate. This means that for most engineering surfaces with random roughness, the minimum cavity radius predicted by Hsu is the most important size, which can also be predicted using Eq. (2) with $r_e^* = r_c$. It can be concluded based on this study that the models based on cavity geometry and wettability agrees with the Hsu model in predicting the minimum cavity radius. The wettability models (phase stability-based) have an additional advantage, which is the possibility of predicting or incorporating the cavity geometry (radius and depth).

The above models may be validated using artificial nucleation sites.

Qi and Klausner [21] investigated heterogeneous nucleation from artificial cylindrical cavities fabricated on a silicon substrate using water (contact angle 21) and ethanol (contact angle nearly zero). Seven inline cavities with diameter 20 – 60 μm and 45 μm depth were fabricated in the same substrate with cavity spacing 4 mm. It was found that, for water, the measured superheat was about 100 % larger than that predicted using Eq. (2) with $r_e^* = r_c$ and reasonable agreement was obtained when $r_e^* = 0.5r_c$. For ethanol, the wall superheat reached 60 K without observing any bubbles. This disagreement with Eq. (2) may be attributed to the following reasons: (i) the cavities are not deep enough, e.g. the aspect ratio range in their study was 0.75 – 2.25. Using Bankoff criterion in Fig. 4 for water with contact angle $21^0$, the required minimum aspect ratio is 3 while for ethanol with contact angle $6^0$ (as an example) the required aspect ratio is 9.6. (ii) the authors observed significant nucleation sites instability. This instability may affect the measured average wall superheat, which is used to evaluate Eq. (2). (iii) in the case of ethanol, because the contact angle was nearly zero, the cavities may be flooded with liquid. Yu et al. [33] investigated pool boiling of FC-72 on silicon substrate with a 2D array of artificial cylindrical cavities of diameter 200, 100, 50 μm and depth 200, 110 μm. The boiling curve plotted for a surface with cavity diameter 200 μm and depth 110 μm (aspect ratio 0.55) indicated that boiling incipience occurred at 30.5 K while it was 45.9 K for the plain surface. Because the Lorenz model is applicable for conical cavities, the Hsu model will be used to validate these values of the measured superheat. Using the superheat value of the smooth surface (45.9 K), the predicted cavity radius will be about 70 nm which agrees with the random microstructure of the smooth silicon substrate. On the contrary, with artificial cavity radius of 100 μm, Eq. (2) predicts 0.05 K superheat while the Hsu model predicts 10 K superheat. These values are much lower than the experimentally measured value (30.5 K). The reasons of this discrepancy are not understood. It may be due to the fact that the above theories were based on a single nucleation site without taking the effect of thermal interaction among cavities into account. Additionally, the measured superheat is the average value not the local value. Hutter et al. [34] investigated bubble interaction in saturated boiling of FC-72 from artificial cylindrical cavities (D = 10 μm and depth 40 – 100 μm) with integrated sensors beneath each cavity. Their experimental setup can be used to validate the nucleation theories. However, they did not record the exact wall superheat at boiling incipience. Instead, they started boiling by increasing the heater temperature then reduced the heater temperature to the minimum value for a stable bubble growth. This minimum superheat value was found to be 1.3 K for all cavities. The equilibrium superheat predicted using Eq. (2) is 0.9 K and by the Hsu model is 1 K, which are very close to the experimental value (1.3 K). This may raise a question about the definition of the incipient superheat. Is it the wall superheat at the onset of bubble formation or is it the minimum superheat required for the cavity to stay active? It is worth mentioning that the measurements by Hutter et al. may be within the hysteresis loop (in the decreasing direction of heat flux). In other words, the bubble may disappear at this superheat value (1.3 K) if it was given longer time.

In conclusion, it is clear that although boiling incipience models have been developed many years ago, the models lack experimental validation, which is a big challenge. In most cases, the boiling incipience superheat was detected from the slope change of the boiling curve which was constructed based on the average superheat. Additionally, the surface structure was characterized using either SEM images or roughness profile without linking the measured superheat with surface microstructure. The SEM images give only a qualitative description of the surface. The big challenge in validating these theories is to design a surface with cavities of known geometry and measure the local superheat around the cavity. Indeed, there are many studies that measured the local superheat using integrated temperature sensors during single bubble nucleation and growth. Unfortunately, these researchers focused only on bubble dynamics and thus they triggered one single bubble using different techniques such as dialysis sensor, spot radiation heating, laser heating. They did not record or report on the wall superheat at boiling incipience. Few studies tested artificial cavities but again their focus was on bubble dynamics and interaction. Thus, more fundamental work is still required to understand and validate the heterogeneous nucleation theories, which is the first step in designing an efficient boiling surface. However, the research community should agree first on the definition of the incipience superheat, i.e. agree if this should be the superheat recorded with increasing heat flux when the first bubble appears or the minimum wall superheat recoded with decreasing heat flux after activating the nucleation site.

## Models of bubble growth and departure

### *Bubble growth models*

In the above sections, the conditions required to activate nucleation sites were presented and discussed. To continue with the design of boiling heat transfer surfaces, it would be useful to understand the characteristics of bubble growth and departure. It is well known that bubbles grow due to hydrodynamic forces (inertia-controlled) and evaporation at the bubble surface (heat transfer-controlled). The inertia-controlled growth dominates only the early stages of bubble growth (for few microseconds). Additionally, there is agreement among researchers on that the bubble radius is proportional to time ($R \propto t$) in the inertia-controlled growth while it is proportional to the square root of time ($R \propto \sqrt{t}$) in the heat transfer-controlled growth. Many researchers [35–42] investigated bubble growth in a uniform temperature field. Table 1 summarizes the proposed models by these researchers. Although they have adopted different approaches, they all agreed that the heat transfer-controlled growth regime can be expressed as: $R(t) = CJa\sqrt{\alpha t}$. In most models, the transient heat conduction equation was solved for a semi-infinite flat plate rather than a sphere. Thus, the constant $C$ was introduced to account for the spherical geometry of the bubble. Fig. 18 shows a comparison among these models and indicates that there is a good agreement between all models except the models by Fritz and Ende [35] and Prisnyakov [41]. These two models were based only on the energy equation, i.e. the momentum equation was not included. Note that the models by Plesset and Zwick [37], Birkhoff et al. [38], and Scriven [39] are exactly the same (they conducted their own analysis and got the same relation) and the difference between these models and the model by Mikic et al. [42] is insignificant. Also, there is no difference between the models by Zuber [40] and Forster and Zuber [36].

The above models may not be applicable to non-uniform

**Table 1**
bubble growth rate in uniformly superheated liquid.

| Author | Model equations |
|---|---|
| Fritz and Ende [35] | $R = (2/\sqrt{\pi})Ja\sqrt{\alpha t}$ |
| Forster and Zuber [36], Zuber [40] | $R = \sqrt{\pi}Ja\sqrt{\alpha t}$ |
| Plesset and Zwick [37] | $R = \left(\sqrt{12/\pi}\right)Ja\sqrt{\alpha t}$ |
| Birkhoff et al. [38] | $R = \left(\sqrt{12/\pi}\right)Ja\sqrt{\alpha t}$ |
| Scriven [39] | $R = \sqrt{\frac{12}{\pi}}\left\{\frac{\Delta T_{sup}}{\frac{\rho_v}{\rho_l}\left[\frac{h_{fg}}{c_{pl}} + \frac{(c_{pl}-c_v)\Delta T}{c_{pl}}\right]}\right\}\sqrt{\alpha t}$ or $R \cong \sqrt{\frac{12}{\pi}}Ja\sqrt{\alpha t}$ |
| Prisnyakov [41] | $R = \frac{4}{3\sqrt{\pi}}Ja\sqrt{\alpha t}$ |
| Mikic et al. [42] | $R^+ = \frac{2}{3}\left[(t^+ + 1)^{3/2} - (t^+)^{\frac{3}{2}} - 1\right] A = \left(\frac{2}{3}\frac{\rho_v h_{fg}\Delta T}{\rho_l T_{sat}}\right)^{0.5} B = \sqrt{\frac{12\alpha}{\pi}}Ja$ <br> $R^+ = \frac{RA}{B^2}t^+ = \frac{tA^2}{B^2}$ |

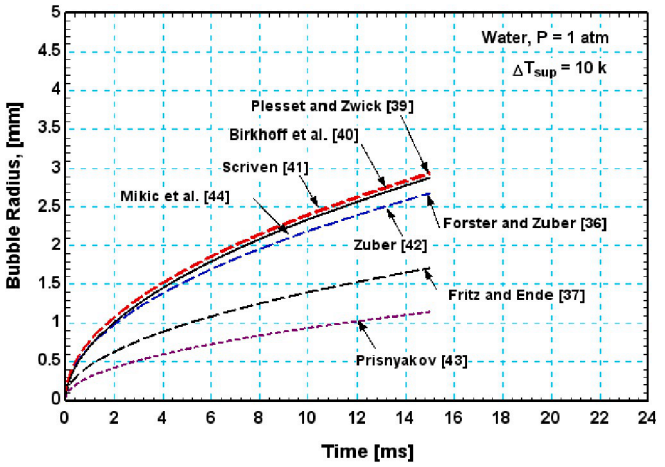


**Fig. 18.** Comparison between models of bubble growth in a uniformly superheated liquid.

temperature fields (bubble growth on a heated surface) and therefore several models were proposed based on the following three mechanisms: (i) bubble growth due to microlayer evaporation (MLE), (ii) bubble growth due to evaporation from the thermal boundary layer surrounding the bubble surface, i.e. relaxation layer evaporation (RLE), (iii) combination of MLE and RLE. Table 2 summarizes the proposed theoretical and empirical model equations proposed by researchers for bubble growth at a heated surface, which are compared in Fig. 19. The model by Zuber [40] requires a value for the applied heat flux. For the sake of comparison, the heat flux was predicted using the Cooper [43] heat transfer correlation for the same superheat value of 10 K as used for the rest of the models. It is obvious that there is no general agreement on the prediction of bubble growth rate in a non-uniform temperature field. Some models predict low growth rate such as the models by [41,44,45]. The model by Mikic and Rohsenow [46] depends on the waiting time, which was calculated here using the model by Han and Griffith [29]. It is worth noting that the waiting time by this model depends on the cavity radius. Thus, the prediction of bubble growth rate was conducted for cavity radius 10 and 100 μm. This model predicts that the bubble growth rate increases significantly with increasing the cavity size. The bubble growth model by [29] depends also on the cavity size but the growth rate increases slightly with increasing cavity radius. The model by Du et al. [47], which was based on dimensional analysis agrees well with Zuber [40] and Mikic and Rohsenow [46] for 100 μm cavity radius. The model by Chen et al. [48] which was based on micro-layer evaporation agrees well with Cooper [49], which combines microlayer evaporation and evaporation from the relaxation layer.

*Bubble departure models*

Fig. 20 shows the bubble departure diameter versus wall superheat predicted using different models, which are summarized in Table 3. The comparison was conducted using water at atmospheric pressure. The figure demonstrates that the models can be divided into three groups. The first group [45,50–54,69] predicts constant value of departure diameter, the second group [55 –59] predicts diameter that increases moderately with superheat, and the third group [60 –66] predicts diameter that increases strongly with increasing superheat. The figure indicates also that the predicted bubble departure diameter at 10 K

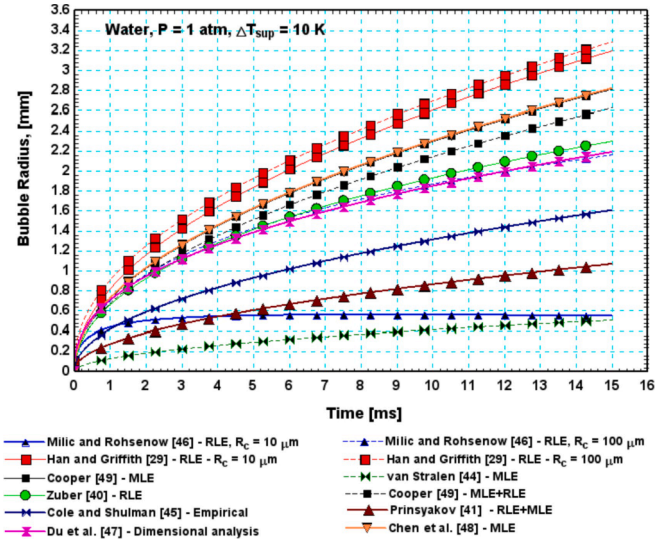


**Fig. 19.** Comparison between bubble growth models for non-uniform temperature field.

**Table 2**
Bubble growth rate in a non-uniform temperature field.

| Author | Model equations |
|---|---|
| Zuber [40] | $R = b\frac{2}{\sqrt{\pi}}Ja\sqrt{\alpha t}\left[1-\frac{q\sqrt{\pi\alpha t}}{2k\Delta T}\right] b = 1 to \sqrt{3}\ b = \pi/2$ was recommended |
| Han and Griffith [29] | $R = r_c + \frac{\varphi_s\varphi_c}{\varphi_v}\frac{\rho c\alpha}{\rho_v h_{fg}}\left[\frac{2(T_w - T_{sat})\sqrt{t}}{\sqrt{\pi\alpha}} - \frac{T_w - T_\infty}{\delta_{th}}\frac{\delta_{th}^2}{4\alpha}\left(\frac{4\alpha t}{\delta_{th}^2}erf\frac{\delta_{th}}{\sqrt{4\alpha t}} + \frac{2}{\sqrt{\pi}}\frac{\sqrt{4\alpha t}}{\delta_{th}}\exp\left[-\frac{\delta_{th}^2}{4\alpha t}\right] - 2erfc\frac{\delta_{th}}{\sqrt{4\alpha t}}\right) + \frac{\varphi_b h_v(T_w - T_{sat})t}{\varphi_v\rho_v h_{fg}}\right]$ $\varphi_s = 0.5(1+\cos\theta)$, $\varphi_b = 0.25 sin^2\theta$, $\varphi_v = 0.25(2+\cos\theta(2+sin^2\theta))$ |
| Cole and Shulman [45] | $R = 2.5Ja^{0.75}\sqrt{\alpha t}$ |
| Cooper [49] | Microlayer evaporation:For high conductivity wall/low conductivity liquid: $R = 2.5Pr^{-0.5}Ja\sqrt{\alpha t}$For low conductivity wall/high conductivity liquid: $R = 1.12\sqrt{\frac{\rho_w c_w k_w}{\rho_l c_{pl} k_l}}Ja\sqrt{\alpha t}$Evaporation from the microlayer and the bubble surface:$R = 0.8\sqrt{3Pr/\pi}\left\{2.5\sqrt{\nu}\ \frac{\Delta T_b}{\psi}\right\}t^{0.5} + \left(2.5\sqrt{\nu}\ \frac{\Delta T_{sup}}{\psi}\right)t^{0.5}\Delta T_b = T_{bulk} - T_{sat}$ |
| Mikic and Rohsenow [46] | $R = \sqrt{\frac{12}{\pi}}Ja\sqrt{\alpha t}\left[1-\frac{\Delta T_w - \Delta T_b}{\Delta T_w}\left\{\left(1+\frac{t_w}{t}\right)^{0.5} - \left(\frac{t_w}{t}\right)^{0.5}\right\}\right]$ |
| Prisnyakov [41] | $R = R_0 + \frac{2}{3}f_\theta Ja\left(\frac{2}{\sqrt{\pi}}\sqrt{\alpha t} + fNt\right), f_\theta = \frac{(1-\cos\theta)}{1+0.5\cos(2+sin^2\theta)}, N = \frac{q}{\rho_l c_l \Delta T} f = 0.5(1-\cos\theta)$ |
| Van Stralen et al. [44] | $R = 0.47(1/\sqrt[3]{2})Pr^{-1/6}Ja\sqrt{\alpha t}$ |
| Chen et al. [48] | $R = \left(\frac{C}{\phi f(C)}Ja\right)^{0.5}\sqrt{\alpha t}\phi = \frac{f(C)C_1^2 Pr}{C^3 Ja}, C = \frac{R_b}{R}f(C) = 1-0.75\left(1-\sqrt{1-C^2}\right)^2 + 0.25\left(1-\sqrt{1-C^2}\right)^3$ C was taken from Mei et al. (1995):$C = \left[(0.4134Ja^{0.1655})^{-6} + (1-0.1\exp(-0.0005Ja))^{-6}\right]^{-1/6} C_1 = 0.00525Ja^{0.752}Pr^{-0.5}(k_l/k_s)^{-0.113}(\alpha_l/\alpha_s)^{-0.117}$ |
| Du et al. [47] | $R = 2.1077Ja^{0.7902}\sqrt{\alpha t}^n$[mm], $n = 1.0012e^{-P/0.3257} - 0.9624e^{-\frac{P}{0.6161}} + 0.5$ , $P$ in MPa |

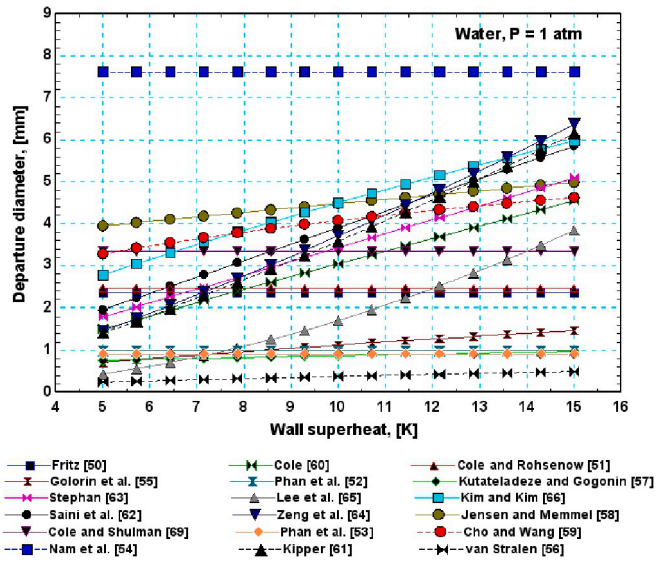


**Fig. 20.** Comparison between bubble departure diameter predicted using existing models.

superheat ranges from 0.9 to 7.6 mm. The reasons of this wide scatter are not clearly understood but possible reasons could be the following: (i) difference in experimental thermal boundary conditions, i.e. constant heat flux versus constant surface temperature. Some researchers studied bubble dynamics using transparent substrates with integrated micro-sensors to control the surface temperature. Conducting the test under constant surface temperature may result in different behaviour compared to constant heat flux boundary conditions. (ii) difference in surface microstructure and material. (iii) uncertainty in the measurement of diameter especially when the bubble shape is deformed. (iv) definition of the equivalent bubble diameter. (v) experimental methodology. For example, Surtaev et al. [32] investigated bubble dynamics of saturated boiling of water and ethanol on transparent sapphire substrate (20 × 20 × 0.4) mm. Although boiling started at 90 kW/m$^2$ and 37 kW/m$^2$ for water and ethanol, respectively, the bubble dynamics were presented for heat flux values much smaller than these values (31.5 kW/m$^2$ for water and 33.6 kW/m$^2$ for ethanol). This means that the bubble dynamics were measured after activating the nucleation sites at high heat fluxes, i.e. the measurements were conducted with decreasing heat flux in the hysteresis zone. This might raise the question whether the results will be the same in the increasing mode or not.

*Effect of wettability and fluid on bubble dynamics*

In this section, the bubble departure models that took into account the effect of cavity size will be used to help understand the effect on surface design. Chesters [67] predicted the bubble shape based on a balance between pressure, gravity, and surface tension forces. He concluded that the bubble departure diameter depends on the bubble growth mode, i.e. confined versus spreading mode. In the confined mode, the bubble grows while the TPL stays anchored to the cavity edges while in the spreading mode, the contact line spreads beyond the cavity edges. He gave a criterion for the transition from the confined to the spreading growth mode, which depends on fluid properties and static contact angle. If the static contact angle is greater than a critical value, the bubble will spread over the surface during its growth before it shrinks and form a neck at departure. The critical angle was given as:

$$\sin\theta_{crit} = \frac{4\times 2^{1/4}}{3}\sqrt{\frac{r_c}{(\sigma/g\Delta\rho)^{0.5}}} \tag{8}$$

In the above equation, $r_c$ is the critical cavity radius above which spreading growth mode occurs for a fluid with contact angle $\theta$. This equation indicates that for a fixed cavity radius of 20 μm as an example, the critical angle for water, HFE-7100 and FC-72 is 8.1$^0$, 13$^0$ and 15.4$^0$, respectively. Because the contact angle of water with most surfaces is larger than the critical angle, the TPL is expected to spread beyond the cavity mouth, i.e. larger contribution from the microlayer evaporation and larger dry area underneath the bubble at high heat fluxes. In this case, the bubble departure diameter was found to be independent of the cavity size and the obtained equation was the same as the one proposed by Fritz [50], see Table 3. On the contrary, the contact angle of highly wetting fluids (around zero) is always less than the critical angle. Thus, the TPL stay anchored to the cavity mouth and the bubble departure diameter depends on the cavity size. It increases as the cavity size increases. For this case, Chesters [67] gave Eq. (9) below for the prediction of bubble departure diameter. In both modes of bubble growth, the bubble forms a neck at the moment of departure and shrinks with a minimum contact area with the surface. The contact radius was given by Eq. (10) for the confined growth mode and Eq. (11) for the spreading growth mode.

**Table 3**
Models and correlations of bubble departure diameter.

| Author | Models equations |
|---|---|
| Saini et al. [62] | Ja less than 16: $\left(\frac{g}{\alpha_l^2}\right)^{1/3} D_d =$ $1.35Ja^{4/3}\left[1.22+\sqrt{1+2.67\frac{c_l\sigma\Delta T}{\alpha_l q Ja^4}}\right]^{2/3}$ $16 < \mathrm{Ja} < 100$: $\left(\frac{g}{\alpha_l^2}\right)^{1/3} D_d = 9.18Ja$Ja $> 100$: $\left(\frac{g}{\alpha_l^2}\right)^{1/3} D_d = \left(6.6\frac{c_p\Delta T\sigma}{\alpha_l q}\right)^{1/3}$ |
| Fritz [50] | $D_d = 0.0208\theta\sqrt{\sigma/g\Delta\rho}$θ: 35 for organics and 45 for water – in degree |
| Cole and Shulman [69] | $D_d = 0.0208\theta\sqrt{\sigma/g\Delta\rho}\left[1+0.0025(dD/dt)^{1.5}\right]$ |
| Cole [60] | $D_d = 0.04Ja\sqrt{\sigma/g\Delta\rho}$ |
| Cole and Rohsenow [51] | $D_d = CJa^{*5/4}\sqrt{\frac{\sigma}{g\Delta\rho}}$,C = 0.00015 for water and 0.000465 for other fluids,$Ja^* = \frac{\rho_l c_l T_C}{\rho_v h_{fg}}$ |
| Kiper [61] | $D_d = 2.7Ja^{4/3}\left(g/\alpha^2\right)^{-1/3}$ |
| Van Stralen et al. [56] | $D_d = 2.63(1/g)^{1/3}Ja^{2/3}\alpha^{2/3}\left(1+\sqrt{2\pi/3Ja}\right)^{0.25}$ |
| Golorin et al. [55] | |
| Stephan [63] | $D_d = 0.25\left[1+\left(\frac{Ja}{Pr}\right)^2\frac{100000}{Ar}\right]^{0.5}\sqrt{\frac{2\sigma}{g\Delta\rho}}$,$Ar = \left(\frac{\rho_l g\Delta\rho}{\mu_l^2}\right)\left(\sqrt{\frac{\sigma}{g\Delta\rho}}\right)^3$ |
| Kutateladze and Gogonin [57] | $D_d = 0.25\left[(1+10^5K1)\frac{\sigma}{g\Delta\rho}\right]^{0.5}$ $K1 < 0.06$,$K1 = \frac{Ja}{Pr}\left\{\left(\frac{\rho_l g\Delta\rho}{\mu_l^2}\right)\left(\frac{\sigma}{g\Delta\rho}\right)^{3/2}\right\}^{-1}$ |
| Jensen and Memel [58] | $D_d = 0.91\left[1.8+10^5K1\right]^{2/3}\sqrt{\sigma/g\Delta\rho}$ |
| Zeng et al. [64] | $D_d = 2\left[\frac{3k^{2/n}}{4g}(10n^2+n(n-1))\right]^{2/(2-n)}$ |
| Lee et al. [65] | $D_d = 2\left[\frac{25}{2}\sqrt{27}Ja\alpha\sqrt{\frac{\rho_l}{\sigma}}\right]^2$ |
| Kim and Kim [66] | $D_d = 0.1649Ja^{0.7}\sqrt{\frac{\sigma}{g\Delta\rho}}$ |
| Phan et al. [52] | $D_d = 0.627\frac{2+3\cos\theta-\cos^3\theta}{4}\sqrt{\frac{\sigma}{g\Delta\rho}}$,$\theta \le 90$ |
| Phan et al. [53] | $D_d = \left(6\sqrt{\frac{3}{2}}\right)^{1/3}\left(\frac{\rho_l}{\rho_v}\right)^{-0.5}\left(\frac{\rho_l}{\rho_v}-1\right)^{1/3}(\tan\theta)^{-0.25}\sqrt{\frac{\sigma}{g\Delta\rho}}$ |
| Nam et al. [54] | $D_d = \sqrt{\frac{24\sin^2\theta}{2+3\cos\theta-\cos^3\theta}}\sqrt{\frac{\sigma}{g\Delta\rho}}$ |
| Cho and Wang [59] | For $t^+ \ge 5: D_d = 0.652\theta^{0.581}\Delta T^{0.313}La$For $t^+ < 5: D_d = La\sqrt{\frac{24\sin^2\theta}{2+3-\cos^3\theta}}$, $t^+ = \frac{\theta\sigma^{0.5}\rho_L^{1/3}\Delta T^{1/3}}{g^{1/6}\Delta\rho^{0.5}\nu^{2/3}}$, The contact angle is in radians |

$$R = \left[1.5 r_c \frac{\sigma}{g\Delta\rho}\right]^{1/3} \quad (9)$$

$$r_{contact} = r_c \quad (10)$$

$$r_{contact} = \sqrt{\frac{3}{32}} sin^2\theta \sqrt{\frac{\sigma}{g\Delta\rho}} \quad (11)$$

The size of the contact area is expected to affect the bubble departure size through its effect on the surface tension force, $F_s = 2\pi\sigma r_{contact}$. For water, with $\theta = 60^0$ , the bubble contact radius at departure, calculated using Eq. (11), is 575 μm. For FC-72 with $\theta = 10^0$ in Eq. (8), the critical radius will be 1.7 μm, i.e. confined bubble growth occurs for cavities with radius less than or equal 1.7 μm. In that case, the bubble contact radius equals the cavity radius. Thus, the surface tension force is expected to be much larger in the case of water (low wetting liquid) compared to FC-72 (highly wetting liquid) bearing in mind also that the surface tension of water is much larger than FC-72.

To get an idea about the effect of heat flux, system pressure, wettability and fluid on bubble dynamics, a force balance model by Zeng et al. [64] is used in this section. The interested reader is referred to [64] for more details on the model equations. In their model, they ignored the surface tension force at the moment of bubble departure due to the necking phenomenon and assumed that buoyancy and drag are the important forces. In this section, the model by Zeng et al. was used but the surface tension force was taken into consideration. The bubble contact diameter required for the calculation of surface tension force was obtained from Eq. (10) and (11) given above by Chesters [67]. The bubble growth time was estimated from the bubble growth model by Forster and Zuber [36], see Table 1, and the Zeng et al. bubble departure model. The waiting time required to calculate the frequency was estimated roughly from the transient heat transfer model by Han and Griffith [28], $t_w = \delta_{th}^2/\pi\alpha_l$. The required thermal boundary layer thickness was calculated from $\delta_{th} = k_l/h_{tp}$ and the two-phase heat transfer coefficient was estimated using the Cooper [43] correlation. The wall superheat required for the bubble growth rate was estimated from $\Delta T_{sup} = q/h_{tp}$. Fig. 21 illustrates the effect of heat flux and type of fluid on bubble departure diameter predicted using the Zeng et al. model. It indicates that the bubble departure diameter increases moderately with increasing heat flux (wall superheat) and the departure diameter of water was significantly larger than that of FC-72 and HFE-7100. For water with $\theta = 10^0$, the departure diameter increased from 0.83 to 2.6 mm in the heat flux range 10 – 300 kW/m$^2$. For FC-72, the diameter increased from 0.27 to 1.07 mm while it increased from 0.32 to 1.02 mm for HFE-7100 for the same heat flux range. Increasing the contact angle of water to $60^0$ results in significant increase in the departure diameter where it increased from 3.66 to 4 mm. Yu and Lu [68] measured the departure diameter of FC-72 bubble for heat fluxes up to 95 kW/m$^2$ and reported values ranging from 0.2 to 0.5 mm, which agrees very well with the current calculations. Comparing the bubble growth rate and growth time in Fig. 22 at the wall superheat 10 K and the same contact angle, $\theta = 10^0$ indicates that bubble grows faster in the case of water with larger growth time compared to FC-72 and HFE-7100. For water, the predicted growth time is 3.05 ms while it was 1.56 ms and 2.19 ms for FC-72 and HFE-7100. Increasing the contact angle for water from $10^0$ to $60^0$ (by coating as an example) resulted in significant increase in bubble growth time, e.g. it reached 17.9 ms. The reason of larger growth time in case of water could be due to the much larger bubble contact area in case of water as discussed above. This results in larger surface tension force which keeps the bubble attached to the surface until the buoyancy and other forces overcome the surface tension force. It is worth mentioning that Jackob number (*Ja*) and liquid thermal diffusivity of water at the same superheat are above 100 % and 400 % larger, respectively compared to FC-72 and HFE-7100. The larger the *Ja* and diffusivity, the larger the bubble growth rate and departure diameter. It is important to note that the larger the bubble growth rate (large growth velocity), the larger the chance of microlayer formation (trapping liquid film underneath the bubble). This may explain why the contribution of microlayer evaporation mechanism is large in case of water (66 % as in ref. [2]) compared to FC-72 (16.3 – 28.8 % as in ref. [1]).

Fig. 23 illustrates the effect of heat flux and fluid on bubble departure frequency. For the same heat flux and contact angle, the bubble departure frequency of HFE-7100 is slightly larger than that of FC-72 but both are significantly larger than water. In case of highly wetting fluids, the frequency increases rapidly with heat flux up to certain heat flux value after which the frequency reaches an asymptotic value. It is interesting to note that this heat flux value is about 200 kW/m$^2$, which is very similar to the critical heat flux values of these two fluids discussed in Part II [10]. On the contrary, the frequency increases almost linearly with heat flux in case of water. Additionally, reducing the contact angle from $60^0$ to $10^0$ in case of water resulted in significant increase in bubble frequency. This might explain the enhancement in heat transfer with water in hydrophilic and super-hydrophilic surfaces compared to hydrophobic surfaces as will be discussed in Part II [10]. Fig. 24 depicts the effect of pressure and wettability on departure diameter and frequency. It shows that the effect of pressure on departure diameter and frequency depends on wettability. In case of very high wettability, the departure diameter decreases continuously with increasing pressure while the frequency increases continuously with increasing pressure. When the wettability decreases (increasing contact angle), the departure diameter decreases with increasing pressure up to a certain pressure value (slightly above the atmospheric pressure) after which the diameter does not change significantly. With decreasing wettability, the frequency

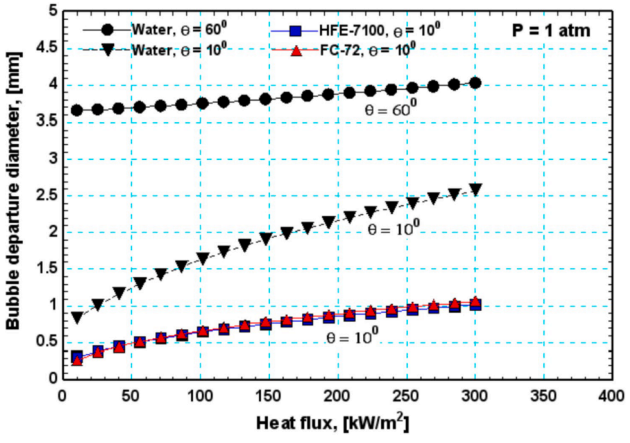


**Fig. 21.** Effect of heat flux and type of fluid on bubble departure diameter.

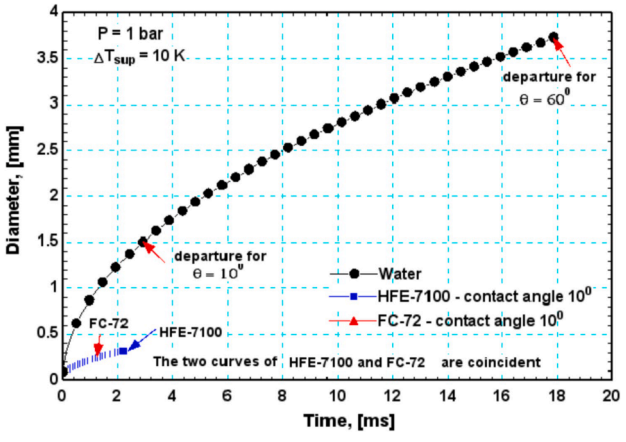


**Fig. 22.** Effect of fluid on bubble growth rate and growth time, the arrow refers to the moment of departure.

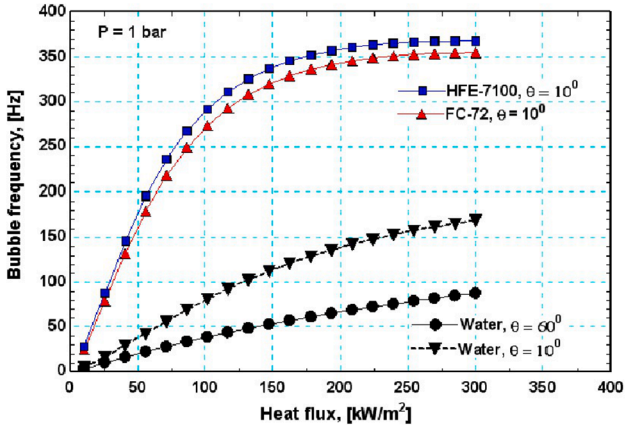


**Fig. 23.** Effect of heat flux and fluid on bubble departure frequency.

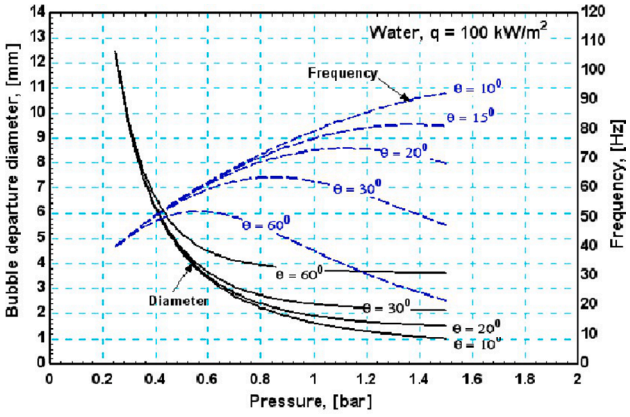


**Fig. 24.** Effect of system pressure and wettability on departure diameter and frequency.

increases to a maximum value after which it decreases continuously with increasing pressure. This figure may explain why the heat transfer rate increases with pressure in some studies while there was no effect or adverse effect in some other studies.

It can be concluded from section 3 that there is a wide scatter among the results of past researchers on the prediction of bubble growth rate and departure diameter. This could be due the following reasons: (i) there is no general agreement on the heat transfer mechanism contributing to the bubble growth, e.g. microlayer evaporation, evaporation from the relaxation layer, combined evaporation from microlayer and relaxation layer; (ii) differences in microstructure and wettability. For moderate wettability case, the bubble can spread beyond the cavity diameter and trap a thin liquid layer underneath the bubble, which can contribute to bubble growth significantly. For highly wetting liquids, the bubble remains anchored to the cavity mouth without spreading (small contact area with the surface), i.e. more contribution from the relaxation layer. In case of hydrophobic surfaces, the bubble spreads on the surface with a dry patch underneath and thus evaporation is limited to the bubble cap. (iii) difference in substrate material and heating method. The substrate material (heated transparent materials versus metallic materials) affects the microstructure and wettability. In some studies, integrated heaters/sensors were used with thin test sections, while in some others large metal blocks were tested. The parametric analysis conducted in this study for bubble dynamics indicated the following: (i) the bubble departure diameter increases with increasing heat flux and contact angle. (ii) The bubble growth rate and growth time of water are significantly large compared to highly wetting liquids. (iii) The bubble growth time increases with increasing contact angle. (iv) For the same heat flux and contact angle, the bubble departure frequency of water was significantly lower than that of highly wetting liquids. (v) For the same fluid and heat flux, the frequency decreases as the contact angle increases. (vi) The bubble departure diameter decreases with increasing pressure but the effect of pressure on frequency depends on wettability.

## Conclusions

In Part I of this two-part paper we presented a thorough discussion and analysis of the fundamental knowledge required for the design of boiling surfaces. The fundamentals of heterogeneous nucleation, prediction of the incipience superheat and bubble dynamics parameters were discussed while highlighting the effect of fluid properties and wettability. The major conclusions of this work are given below:

1. The gas entrapment criterion given by Bankoff [12], with the static contact angle as a parameter, is recommended for the design of boiling surfaces with stable nucleation sites.
2. Although the heterogeneous nucleation theories have been developed many years ago (dates back to 1960 s), these theories are not well-validated. The commonly adopted models were the thermal layer-based models and the phase instability-based models. The fundamental differences between these models are: (i) All the thermal layer-based models did not take the effect of wettability into consideration while wettability is included only in the instability-based models. (ii) All the thermal layer-based models recommend that the cavity mouth diameter is the only geometrical parameter required to predict the incipience superheat. On the contrary, the instability-based models recommend the cavity mouth diameter and cavity depth. (iii) For a fixed wall superheat, the thermal layer-based models predict that there is a range of active cavities with diameter between a minimum and maximum value. This maximum value didn't match the values obtained from the surface analysis. The maximum and minimum cavity diameter resulted from a solution of a quadratic equation that has two solutions (are the two solutions valid or one should be rejected?). The instability-based models could predict a range of cavity sizes for a fixed superheat value (similar to the thermal layer-based models) due to difference in wettability, cavity diameter and depth. The maximum value in this range matches the surface measurements (more realistic). Thus, validation of the incipient superheat theories is difficult without precise surface characterization, measuring the local superheat near the cavity and understanding the change in wettability with temperature
3. Based on the phase instability-based models, the effect of wettability on the incipience superheat depends on the cavity cone angle (depth). The models predict that the superheat increases as surface tension increases for liquids having nearly the same slope of the vapour-pressure curve. However, there are reports of results with fluids of different surface tension boiling on the same surface and giving an opposite surface tension effect, i.e. lower superheat with fluids of larger surface tension. The effect of surface tension is not thus fully understood. Note that one assumes that in the experiments that relate to this, careful degassing was carried out and all dissolved gasses were completely removed as the presence of some residual dissolved gases can reduce the incipient superheat.
4. Evaluation of bubble growth models indicated that there is agreement on the bubble growth rate in a uniform temperature field, while there is a large scatter on the prediction of bubble growth at the boiling surface.
5. There is no general model for the prediction of bubble departure diameter and there is a large scatter among the existing models. This may be due to the discrepancy on the dominant forces that affect the bubble departure and the use of different bubble growth models. It is worth mentioning that the bubble growth rate (velocity) is required to estimate the drag and inertia forces, which affect the bubble departure diameter.

6. The parametric analysis for bubble dynamics indicated that bubble departure diameter increases with heat flux (wall superheat) and the diameter is larger for liquids with larger Jackob number. As the contact angle increases, the bubble growth time increases due to increased surface tension force. For dielectric liquids (low surface tension), the bubble frequency increases rapidly with heat flux to an asymptotic value while it increased moderately for high surface tension liquids (water). For the same fluid, the effect of system pressure on departure frequency and diameter depends on wettability. For high wettability, the diameter decreases continuously with increasing pressure. As the wettability decreases, the departure diameter decreased from a large value at sub-atmospheric pressure to an asymptotic value at pressures above the atmospheric pressure. Regarding the frequency, for high wettability, the frequency increases with increasing pressure, while as the wettability decreases, the frequency reaches a maximum value then decreases rapidly with increasing pressure. This may explain the complex effect of pressure on the HTC.
7. The design of boiling surfaces is still very challenging and there is a need to test different fluids on the same surface material and microstructure instead of testing one fluid with different random structure. The definition of what is called "cavity" should be agreed among researchers because in most cases surfaces have protrusions rather than holes. Additionally, there is a need for testing metallic surfaces with artificial nucleation sites to validate the existing nucleation theories.

## Declaration of Competing Interest

The authors declare that they have no known competing financial interests or personal relationships that could have appeared to influence the work reported in this paper.

## Acknowledgement

The work described in this paper is based on research work supported by the Engineering and Physical Sciences Research Council, UK (Grant Reference: EP/S019502/1).

## References

[1] S. Moghaddam, K. Kiger, Physical mechanisms of heat transfer during single bubble nucleate boiling of FC-72 under saturation conditions – I, Experimental investigation, Int. J. Heat and Mass Transfer 52 (5–6) (2009) 1284–1294.
[2] S. Narayan, A. Srivastava, S. Singh, Rainbow schlieren-based investigation of heat transfer mechanisms during isolated nucleate pool boiling phenomenon: effect of superheat level, Int. J. Heat and Mass Transfer 120 (2018) 127–143.
[3] Y. Y. Hsu, On the size range of active nucleation cavities on a heating surface, Journal of Heat Transfer, pp. 207 – 213, 1962.
[4] T.G. Karayiannis, M.M. Mahmoud, Flow boiling in microchannels: fundamentals and applications, Appl. Therm. Eng. 115 (2017) 1372–1397.
[5] S. Mori, Y. Utaka, Critical heat flux enhancement by surface modification in a saturated pool boiling: A review, Int. J. Heat Mass Transf. 108 (2017) 2534–2557.
[6] G. Liang, I. Mudawar, Review of pool boiling enhancement by surface modification, Int. J. Heat Mass Transf. 128 (2019) 892–933.
[7] U. Sajjad, A. Sadeghianjahromi, H.M. Ali, C.-C. Wang, Enhanced pool boiling of dielectric and highly wetting liquids - a review on enhancement mechanisms, Int. Commun. Heat Mass Transfer 119 (2020) 104950, https://doi.org/10.1016/j.icheatmasstransfer.2020.104950.
[8] W. Li, R. Dai, M. Zeng, Q. Wang, Review of two types of surface modification on pool boiling enhancement: Passive and active, Renew. Sustain. Energy Rev. 130 (2020) 109926, https://doi.org/10.1016/j.rser.2020.109926.
[9] A. Mehralizadeh, S. Reza Shabanian, G. Bakeri, Effect of modified surfaces on bubble dynamics and pool boiling heat transfer enhancement: A review, Thermal Science and Engineering Progress 15 (2020) 100451, https://doi.org/10.1016/j.tsep.2019.100451.
[10] M.M. Mahmoud, T.G. Karayiannis, Pool boiling review: Part II – heat transfer enhancement, Therm. Sci. Eng. Prog. (2021), https://doi.org/10.1016/j.tsep.2021.101023.
[11] R.N. Wenzel, Resistance of solid surfaces to wettability by water, Ind. Eng. Chem. 28 (1936) 988.
[12] S.G. Bankoff, Entrapment of gas in the spreading of a liquid over a rough surface, A, I. Ch. E. Journal 4 (1) (1958) 24–26.
[13] J.J. Lorenz, The effects of surface conditions on boiling characteristics, PhD, Massachusetts Institute of Technology, 1972.
[14] W. Tong, A. Bar-Cohen, T.W. Simon, S.M. You, Contact angle effects on boiling incipience of highly-wetting liquids, Int. J. Heat and Mass Transfer 33 (1) (1990) 91–103.
[15] R.H.S. Winterton, Nucleation of boiling and cavitation, J. Phys. D: Appl. Phys. 10 (1977) 2041–2056.
[16] K. Cornwell, On boiling incipience due to contact angle hysteresis, Int. J. Heat and Mass Transfer 25 (2) (1982) 205–211.
[17] C.H. Wang, V.K. Dhir, On the gas entrapment and nucleation site density during pool boiling of saturated water, J. of Heat Transfer 115 (1993) 670–679.
[18] M.-H. Shi, J. Ma, B.-X. Wang, Analysis on hysteresis in nucleate pool boiling heat transfer, Int. J. Heat and Mass Transfer 36 (18) (1993) 4461–4466.
[19] D. Gorenflo, U. Chandra, S. Kotthoff, A. Luke, Influence of thermophysical properties on pool boiling heat transfer of refrigerants, Int. J. of Refrigeration 27 (5) (2004) 492–502.
[20] A.V. Pesse, G.R. Warrier, V.K. Dhir, An experimental study of the gas entrapment process in a closed-end microchannels, Int. J. Heat and Mass Transfer 48 (2005) 5150–5165.
[21] Y. Qi, J.F. Klausner, Heterogeneous nucleation with artificial cavities, J. of Heat Transfer 127 (2005) 1189–1196.
[22] P. J. Marto and W. M. Rohsenow, Nucleate boiling instability of alkali metals, J. of Heat Transfer, pp. 183 – 193, 1966.
[23] P.G. Kosky, Nucleation site instability in nucleate boiling, Int. J. Heat and Mass Transfer 11 (5) (1968) 929–932.
[24] S.T. Hsu, F.W. Schmidt, Measured variations in local surface temperatures in pool boiling of water, J. of Heat Transfer 83 (3) (1961) 254–260.
[25] P. Griffith and J. W. Wallis, The role of surface conditions in nucleate boiling, Technical report no. 14, Division of industrial cooperation, Massachusetts Institute of Technology, Cambridge, Massachusetts, December 1, 1958.
[26] S. Dahariya, A.R. Betz, High pressure pool boiling: mechanisms for heat transfer enhancement and comparison to existing models, Int. J. Heat Mass Transfer 141 (2019) 696–706.
[27] S.J. Thiagarajan, R. Yang, C. King, S. Narumanchi, Bubble dynamics and nucleate pool boiling heat transfer on microporous copper surfaces, Int. J. Heat Mass Transfer 89 (2015) 1297–1315.
[28] B. Yu, P. Cheng, A fractal model for nucleate pool boiling heat transfer, J. Heat Transfer 124 (2002) 1117–1124.
[29] H. Chi-Yeh, P. Griffith, The mechanism of heat transfer in nucleate pool boiling – part I: bubble initiation, growth and departure, Int. J. Heat Mass Transfer 8 (6) (1965) 887–904.
[30] A.E. Bergles, W.M. Rohsenow, The determination of forced-convection surface boiling, heat transfer, J. of Heat Transfer 86 (3) (1964) 365–372.
[31] S. G. Kandlikar, V. R. Mizo, M. D. Cartwright, E. Ikenze, Bubble nucleation and growth characteristics in subcooled flow boiling of water, HTD vol. 342, ASME proceedings of the 32nd National Heat Transfer Conference, vol. 4, pp. 11 – 18, 1997.
[32] A. Surtaev, An experimental study of vapour bubbles dynamics at water and ethanol pool boiling at low and high heat fluxes, Int. J. Heat Mass Transfer 126 (2018) 297–311.
[33] C.K. Yu, D.C. Lu, T.C. Cheng, Pool boiling heat transfer on artificial micro-cavity surfaces in dielectric fluid FC-72, J. of Micromechanics and Microengineering 16 (2006) 2092–2099.
[34] C. Hutter, D.B.R. Kenning, K. Sefiane, T.G. Karayiannis, H. Lin, G. Cummins, A. J. Walton, Experimental pool boiling investigation of FC-72 on silicon with artificial cavities and integrated temperature microsensors, Exp. Thermal and Fluid Science 34 (4) (2010) 422–433.
[35] W. Fritz, W. Ende, Über den verdampfungsvorgang nach kinematographischen aufnahmen an dampfblasen, Phys. Zeitschr. 37 (1936) 391–401.
[36] H.K. Forster, N. Zuber, Growth of a vapour bubble in a superheated liquid, J. of Applied Physics 25 (4) (1954) 474–478.
[37] M.S. Plesset, S.A. Zwick, The growth of vapour bubbles in superheated liquids, J. of Applied Physics 25 (4) (1954) 493–500.
[38] G. Birkhoff, R.S. Margulies, W.A. Horning, Spherical bubble growth, The Physics of Fluids 1 (3) (1958) 201–204.
[39] L.E. Scriven, On the dynamics of phase growth, Chem. Eng. Sci. 10 (1-2) (1959) 1–13.
[40] N. Zuber, The dynamics of vapour bubbles in nonuniform temperature fields, Int. J. Heat Mass Transfer 2 (1961) 83–98.
[41] V. F. Prisnyakov, Bubble growth in liquids, Translated from Inzhenero-Fizicheskii, vol. 18, no. 5, pp. 844 – 848, 1970, Plenum Publishing Corporation, New York.
[42] B.B Mikic, W.M Rohsenow, P Griffith, On bubble growth rates, Int. J. Heat Mass Transfer 13 (4) (1970) 657–666.
[43] M.G. Cooper, Saturation nucleate pool boiling – a simple correlation, Institute of Chemical Engineering Symposium Series 86 (1984) 785–793.
[44] S.J.D. van Stralen, M.S. Sohal, R. Cole, W.M. Sluyter, Bubble growth rate in pure and binary systems: combined effect of relaxation and evaporation microlayers, Int. J. Heat Mass Transfer 18 (1975) 453–467.
[45] R. Cole, H.I. Shulman, Bubble growth rates at high Jakob numbers, Int. J. Heat Mass Transfer 9 (1966) 1377–1390.
[46] B. Mikic, W. Rohsenow, Bubble growth rates in non-uniform temperature field, Progress in Heat and Mass Transfer II (1969) 283.
[47] J. Du, C. Zhao, H. Bo, A modified model for bubble growth rate and bubble departure diameter in nucleate pool boiling covering a wide range of pressure, Appl. Therm. Eng. 145 (2018) 407–415.

[48] W.C. Chen, J.F. Klausner, R. Mei, A simplified model for predicting vapour bubble growth rates in heterogeneous boiling, J. of Heat Transfer, Transactions of the ASME 117 (1995) 976–980.
[49] M.G. Cooper, A.J.P. Lloyd, The microlayer in nucleate pool boiling, Int. J. Heat Mass Transfer 12 (8) (1969) 895–913.
[50] W. Fritz, Berech des maximal volume von dampf blasen, Phys. Z. 36 (1935) 379–388.
[51] R. Cole, W.M. Rohsenow, Correlation of bubble departure diameters for boiling of saturated liquids, Chem. Eng. Prog. Symp. Ser. 65 (1969) 211–213.
[52] H.T. Phan, N. Caney, P. Marty, S. Colasson, J. Gavillet, Surface wettability control by nanocoating: the effects on pool boiling heat transfer and nucleation mechanism, Int. J. Heat Mass Transfer 52 (2009) 5459–5471.
[53] H.T. Phan, N. Caney, P. Marty, S. Colasson, J. Gavillet, A model to predict the effect of contact angle on the bubble departure radius during heterogeneous boiling, Int. Commun. Heat Mass Transfer 37 (2010) 964–969.
[54] Y. Nam, E. Aktinol, V.K. Dhir, Y.S. Ju, Single bubble dynamics on a superhydrophobic surface with artificial nucleation sites, Int. J. Heat Mass Transfer 54 (2011) 1572–1577.
[55] V.S. Golorin, B.A. Kol'chugin, E.A. Zhakharova, Investigation of the mechanism of nucleate boiling of ethyl alcohol and benzene by means of high-speed motion picture photography, Heat Transfer Sov. Res. 10 (1978) 79–98.
[56] van Stralen, S.J.D., Fundamental developments in bubble dynamics, Proceedings of the 6th Int. Heat Transfer Conf. vol. 6, pp. 429 – 450, 1978.
[57] S.S. Kutateladze, I.I. Gogonin, Growth rate and detachment diameter of a vapour bubble in free convection boiling of a saturated liquid, High Temp. 17 (1979) 667–671.
[58] M.K. Jensen, G.J. Memmel, Evaluation of bubble departure diameter correlations, Prog. 8th Int, Heat Transfer Conf. 4 (1986) 1907–1912.
[59] H. Jeremy Cho, Evelyn N. Wang, Bubble nucleation, growth and departure: a new dynamic understanding, Int. J. Heat Mass Transfer 145 (2019) 118803, https://doi.org/10.1016/j.ijheatmasstransfer.2019.118803.
[60] R. Cole, Bubble frequency and departure volumes at sub-atmospheric pressure, AIChE 13 (1967) 779–783.
[61] A.M Kiper, Minimum bubble departure diameter in nucleate pool boiling, Int. J. Heat Mass Transfer 14 (7) (1971) 931–937.
[62] J.S. Saini, C.P. Gupta, S. Lal, Bubble departure diameter in nucleate pool boiling, Letters in Heat and Mass Transfer 2 (1) (1975) 41–47.
[63] K. Stephan, Saturated pool boiling and sub-cooled flow boiling of mixtures, PhD thesis, University of Auckland, Newzland, 1992.
[64] I.Z. Zeng, J.F. Klausner, R. Mei, A unified model for the prediction of bubble detachment radius in boiling systems-I: pool boiling, Int. J. Heat Mass Transfer 36 (1993) 2261–2270.
[65] H.C. Lee, B.D. Oh, S.W. Bae, M.H. Kim, Single bubble growth in saturated pool boiling on a constant wall temperature surface, Int. J. of Multiphase Flow 29 (2003) 1857–2874.
[66] J. Kim, M.H. Kim, On the departure behaviours of bubble at nucleate pool boiling, Int. J. of Multiphase Flow 32 (2006) 1269–1286.
[67] A.K. Chesters, Modes of bubble growth in the slow-formation regime of nucleate pool boiling, Int. J. of Multiphase Flow 4 (3) (1978) 279–302.
[68] C.K. Yu, D.H. Lu, Pool boiling heat transfer on horizontal rectangular fin array in saturated FC-72, Int. J. Heat Mass Transfer 50 (2007) 3624–3637.
[69] R. Cole, H.L. Shulman, Bubble departure radius at subatmospheric pressure, Chem. Eng. Progr. Symp. Ser. 62 (1966) 6–16.